Resonance Raman and Optical Transient Studies on the Light-Induced Proton Pump of Bacteriorhodopsin Reveal Parallel Photocycles†

W. Eisfeld, C. Pusch, R. Diller, R. Lohrmann, and M. Stockburger*

Max-Planck-Institut für biophysikalische Chemie, Abteilung Spektroskopie, 37018 Göttingen, Germany

Received February 22, 1993

ABSTRACT: The photocycle of bacteriorhodopsin (bR) was studied at ambient temperature in aqueous suspensions of purple membranes using time-resolved resonance Raman (RR) and optical transient spectroscopy (OTS). The samples were photolyzed, and the fractional concentrations of the retinylidene chromophore in its parent state, BR_{570}, and in the intermediate states L_{550}, M_{412}, N_{560}, and O_{640} were determined in the time domain 20 μs–1 s and in the pH range 4–10.5. Two kinetically different L components could be identified. At pH 7 one fraction of L (~65%) decays in 80 μs to M (deprotonation of the Schiff base), whereas the residual part is converted in ~0.5 ms to N. The RR spectra reveal only minor structural changes of the chromophore in the L → N transition. These were attributed to a conformational change of the protein backbone [Ormos, P., Chu, K., & Mourant, J. (1992) *Biochemistry 31*, 6933]. With decreasing pH the L → N transition is delayed to >2 ms following a titration-like function with $pK_a \sim 6.2$. The decay of M_{412} monitored by OTS can be fitted for each pH value by two different amplitudes and time constants (M^f, τ^f; M^s, τ^s; f ≡ fast, s ≡ slow). Both M^f and M^s consist of subcomponents which can be distinguished by their different reaction pathways (but not by OTS). M^f occurs in the reaction sequences L → M^f → N → BR and L → M^f → O → BR. The population of the first sequence, in which N is formed with the time constant τ^f (~2–4 ms, pH 6–10.5), increases with pH. M^s is also found in two different reaction sequences of the form L → M^s → BR. The quantitative analysis reveals that each "titration effect" can be related to a certain fraction of bR. It is proposed that each fraction can be identified with a "subspecies" of bR which undergoes an independent and individual cyclic reaction. A complete reaction scheme is set up which represents the manifold of observed phenomena. It is concluded from the pH dependence of the lifetimes of M^s and N that the reconstitution of BR_{570} in the reaction steps M^s → BR and N → BR requires the uptake of a proton from the external phase. It is argued that this proton catalyzes the reisomerization of retinal, whereas the Schiff base is internally reprotonated from Asp-85. A model for proton pumping is proposed in which the proton taken up from the external phase to catalyze the reisomerization of retinal is the one which is pumped through the membrane during the photocycle of bR.

Bacteriorhodopsin (bR), a retinal-binding protein in the purple membrane of *Halobacteria*, acts as a *light-driven proton pump*. This unique function had first been elucidated by Oesterhelt and Stoeckenius (1973) [for a review, see Stoeckenius and Bogomolni (1982)]. Stimulated by light, bR's retinylidene chromophore, BR_{570}, runs through various intermediate states and, under physiological conditions, is reconstituted within a few milliseconds. Evidently, this cyclic reaction (photocycle) of the chromophore controls the proton pump activity.

Six intermediate states can be characterized by their different kinetic and spectroscopic behavior. By convention they are classified by capitals in alphabetic order according to their appearance time in the photocycle: J_{600} (0.5 ps), K_{590} (5 ps), L_{550} (1–2 μs), M_{412} (80 μs), N_{560} (0.5–3 ms), and O_{640} (2–3 ms). The subscripts denote the respective absorption maxima of the optical spectra in nanometers, and the values in brackets refer to the time constants of appearance under normal conditions (room temperature, neutral pH). It is generally accepted that the primary step from BR_{570} to J involves photoisomerization from the all-*trans* to the 13-*cis* configuration of the retinal chain (Polland et al., 1986; Dobler et al., 1988). All subsequent steps in the photocycle are thermally controlled. With the exception of M_{412}, the imine bond of the chromophore (Schiff base), by which the retinal is linked to the protein backbone, is protonated.

It has been suggested that the step from J to K is due to vibrational relaxation within the chromophore (Doig et al., 1991). The subsequent transition from K to L involves considerable structural rearrangement of the chromophore which might be functionally important (Lohrmann & Stockburger, 1992). During the transition from L to M, the Schiff base becomes deprotonated, a step which is thought to be important for the proton pump mechanism. At the stage of N, the Schiff base is again protonated, but the retinal chain is still in 13-*cis* configuration. Finally, in O the all-*trans* configuration is reestablished, but the chromophore is not yet fully relaxed (Smith et al., 1983). Under normal conditions the parent state BR_{570} is recovered within ~6–8 ms.

In the original work on the photocycle it had been proposed by Lozier et al. (1975) that the various intermediates follow a linear reaction sequence according to their appearance time. However, it turned out that the reaction is more complex. Thus, the decay of M was found to be biphasic with a fast (M^f, τ^f) and a slow (M^s, τ^s) component (Hess & Kuschmitz, 1977; Ort & Parson, 1978; Ohno et al., 1981; Scherrer & Stoeckenius, 1985; Groma & Dancsházy, 1986). For instance, under normal conditions (pH 7, 20 °C) τ^f and τ^s have values of 2.3 and 6.4 ms, respectively, whereas the amplitudes of M^f and M^s are of comparable magnitude (data from the present paper).

† This work was supported in part by the Deutsche Forschungsgemeinschaft.

* To whom correspondence should be addressed.

0006-2960/93/0432-7196$04.00/0

Similarly, it was found by Diller and Stockburger (1988) that the decay of L also occurs with two different time constants.

In an earlier study we had proposed that the complexity of the phenomena in the photocycle might be caused by the existence of slightly different "conformational substates" in which bR undergoes different and independent cyclic reactions (Diller & Stockburger, 1988). A similar proposal was made by Dancsházy et al. (1988). However, it turned out that the kinetic heterogeneity does not correspond to a structural heterogeneity of the chromophore in the parent state. It therefore was proposed by Diller and Stockburger (1988) that it is the protein envelope which exists in various conformational substates which control the reaction steps of the chromophore but do not influence its structure in a spectroscopically detectable way.

It was one of our objectives to prove the "heterogeneous concept" and to make an attempt for a more detailed description of the proposed conformational substates. This notion was introduced by Frauenfelder and his school (Frauenfelder et al., 1988). In the present context we are concerned with a distinct class of fairly stable substates whose lifetime is longer than the period of the cyclic reaction of bR and which therefore may influence the cyclic reaction in a different way. As synonyms for such distinct substates, we use the terms "species" or "subspecies". In any case we restrict the discussion to "functionally active" subspecies.

During the first steps of the photocycle (BR–K–L), the reaction appears to be homogeneous, i.e., each bR molecule undergoes the same reaction pathway with the same first-order rate constants. Only in the period in which the Schiff base donates its proton to the protein environment (L-to-M) or takes up a proton from the protein matrix (M-to-N) does the heterogeneous kinetic behavior become obvious. Experiments on the photocycle therefore should reveal those subspecies which control the internal proton-transfer reactions in a different way.

The proton transfer from and to the Schiff base is not solely controlled by the primary acceptor (this has been identified as the ionized carboxyl side chain of the residue Asp-85; references are given later) or by the proximal donor group. It can rather be assumed that this function is controlled by an ensemble of internal side chains in a cooperative way. Due to a certain degree of flexibility of the proton matrix, it is unlikely that this ensemble has a completely homogeneous structure and "chemical potential" in the whole manifold of bR molecules. Consequently different substructures of this ensemble are conceivable as the basis for the above defined subspecies of bR.

A general strategy to identify functionally active subspecies is to watch the cyclic reactions of bR as a function of an external parameter (e.g., temperature or pH) and to look for inhomogeneous changes in the kinetic behavior. It turned out that in this respect a most useful parameter is the pH of the sample. It is well established that the parent chromophore, BR_{570}, is stable over a wide pH range (pH 3–12). This suggests that the global structure of the protein is not changed in this range. On the other hand, there are numerous reports of a strong pH dependence of transient phenomena in the photocycle. We mention as a typical inhomogeneous behavior that in the range pH 6–9 the amplitudes of M^f and M^s change in the opposite direction as a function of pH (Li et al., 1984; Scherrer & Stoeckenius, 1985). Another interesting observation was that the L-to-M transition is accelerated by a factor of $\sim$10 in the range pH 8–10. This effect could be described by a "titration-like" function with a well-defined apparent pK_a value (Hanamoto et al., 1984; Balashov et al., 1991) and therefore was ascribed to the dissociation of an internal side chain. This suggests that the dissociation of internal side chains may explain at least part of the pH-dependent effects.

In the present work we have studied the pH dependence of the photocycle (pH 4–10) on the time scale between L and the recovery of BR_{570} using time-resolved resonance Raman (RR) and optical transient spectroscopy. Various new pH-dependent phenomena were found which could be described by titration-like functions with apparent pK_a values. In order to decide whether a certain titration effect concerns the entire manifold of bR or only a certain fraction, it was crucial to determine the fractional concentrations of the chromophoric species as a function of time and pH.

Optical transient spectroscopy (flash photolysis) is the most convenient method to study the photocycle of bR. Thus, numerous reports are found in the literature which cover the period between K and the recovery of BR_{570}. In particular we mention those studies in which absorbance changes, $\Delta A(\lambda,t)$, were measured with high precision so that a "global-fit analysis" could be performed (Nagle et al., 1982; Xie et al., 1987; Maurer et al., 1987a,b; Hofrichter et al., 1989; Müller et al., 1991). As a result, one obtains the apparent time constants of the system and their amplitude spectra. Many attempts were made to set up the complete reaction scheme on this basis. However, since the fractional concentrations of the intermediates were not considered, such attempts could not identify a potentially heterogeneous scheme.

This deficiency was overcome by Váró and Lanyi (1991a–c), who inferred the fractional concentrations of BR_{570} and its intermediates as a function of time from the optical difference spectra. This technique is reliable as long as the optical absorption spectra are sufficiently well separated. This, however, is not the case for the intermediate N, whose absorption spectrum ($\lambda_{max} \approx 560$ nm) strongly overlaps with the spectra of BR_{570} and L_{550} (BR_{570} is still the major component in photolyzed samples) so that the fractional concentration of N cannot be obtained with due accuracy. It is obvious that such uncertainties do not allow a correct analysis of those cyclic reactions in which N is involved. This problem can be overcome by using the characteristic vibrational bands in the RR spectra as we have done in the present study.

It was found that the various "titration effects" in our kinetic RR and complementary optical transient studies do not concern the entire manifold of bR molecules but only fractions of it. Each fraction can then be identified with one of the functionally active subspecies which now can be characterized by the pK_a of the respective titration effect. On this basis a complete reaction scheme will be set up in which each of the subspecies undergoes an independent cyclic reaction. It will be shown that homogeneous schemes cannot explain the manifold of observed phenomena in a consistent manner.

Important conclusions on the essential proton-transfer steps in the period between L and the recovery of BR_{570} could be inferred from the complete reaction scheme. The analysis reveals that the basic reaction steps in the different photocycles underlie the same mechanisms. It is proposed that in the reconstitution phase the proton is donated back from Asp-85 to the Schiff base, which contradicts the widely accepted idea that the Schiff base is reprotonated from the cytoplasmic side. It is further concluded that the reisomerization of retinal is catalyzed by a proton which is taken up from the cytoplasmic

side. It is postulated that during the cyclic reaction this proton passes through a hypothetical "internal reactive site" where it initiates the reisomerization of the chromophore and the reconstitution of the protein. It is proposed that this is the proton which is pumped in a single turnover through the membrane. This model is different from the widely accepted model in which the Schiff base acts as an active proton-transfer switch.

MATERIALS AND METHODS

Purple Membranes. Purple membranes (PM) were isolated from *Halobacterium halobium* cells as described by Oesterhelt and Stoeckenius (1974). Samples of PM were provided by the laboratory of D. Oesterhelt (Max-Planck-Institut für Biochemie, Martinsried, Germany). All experiments were performed at 20–23 °C with highly diluted aqueous suspensions of PM, set to an optical density (OD) of 1 at 570 nm (16 μM bR).

Adjustment of the pH. The pH in the PM suspensions was varied in the range 3.5–9 by using a citrate buffer system. The respective pH values were set by adding 0.1 M citric acid at different amounts to 0.1 M Na_2HPO_4. To this solvent was added a highly concentrated suspension of PM at a volume ratio of 1:40 to obtain suspensions of OD = 1 at 570 nm. In the range pH 9–10.5, instead of citric acid, concentrated NaOH was added in small amounts to reach the desired pH values. In a few experiments the solvent was prepared with phosphate buffer (0.1 M KH_2PO_4/Na_2PO_4).

Deviation of Surface from Bulk pH. For the citrate buffer concentrations used, the cation (Na^+) concentration changes from 102 to 165 mM in the range pH 5–7 (Rauen, 1964). Above pH 7, Na^+ quickly approaches the limiting value of 200 mM. From the works of Ehrenberg et al. (1989) and Sheves et al. (1986) it can be estimated by application of the Gouy–Chapman equation that at 136 and 181 mM Na^+ the surface pH values are lower by 0.27 and 0.216 units, respectively, than the bulk values. The difference approaches a value of 0.196 units for 200 mM Na^+.

Pump–Probe RR Experiments. Such experiments were performed with a combination of CW lasers and a flowing sample. For this purpose a spinning cell was used (Figure 1) in which the liquid sample is moved with constant velocity across the laser beams. Since the lateral diffusion of purple membrane patches in the laminar stream is much slower than a full rotational period (T_r) of the cell, the distribution of photoproducts, which follows the intensity profile of the pump beam, remains unchanged during T_r. A delay time, δ, between photolysis in the pump beam and Raman excitation in the probe beam is defined by the lateral distance of the two beams and the flow velocity (v). In all cases, T_r was large compared to the period of the photocycle so that fresh sample always entered the pump beam.

The photochemical decay of the parent chromophore, BR, in a volume element which had passed the center of the pump beam of a Gaussian intensity profile is given by

$$BR = BR_0 \exp[-\bar{l}_B \Delta t_P] \quad (1)$$

with $\bar{l}_B = \gamma_B \sigma_B(\lambda_P) \Phi_P^0 (\pi/8)^{1/2}$ and $\Delta t_P = \bar{d}_P/v$, where the subscripts B and P refer to the parent chromophore and the pump beam, respectively. In these relations, γ_B is the quantum yield of the primary photochemical process, σ_B is the optical absorption cross section, Φ_P^0 is the maximum photon flux density, λ_P is the wavelength, and $\bar{d}_P$ is the $1/e^2$ diameter of the pump beam. $\bar{l}_B$ is the averaged value for the photochemical rate coefficient in the beam, and Δt_P is the residence time of a sample element within the diameter $\bar{d}_P$ [for more details, see Schneider et al. (1989) and Lohrmann et al. (1991)]. The degree of photolysis is determined by the product $\bar{l}_B \Delta t_P$, which is sometimes called the "photoconversion parameter". In order to obtain RR spectra of the intermediates with good quality, a sufficiently high degree of photolysis is required, i.e., $\bar{l}_B \Delta t_P \geq 1$. On the other hand, unwanted secondary photoreactions of intermediates would perturb the kinetic analysis. To meet these requirements, we have used pump beams in the red at 647 nm (krypton laser, Coherent CR 2000) or at 633 nm (He–Ne laser, Spectra Physics 125) where photoreactions of the green- and blue-absorbing intermediates L, N, and M can be largely neglected.

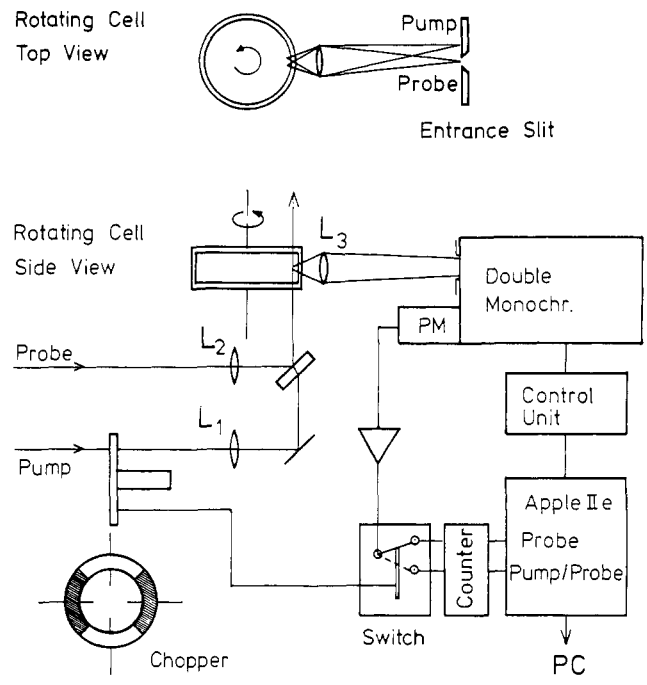

FIGURE 1: Optical layout of a pump–probe Raman experiment. Time resolution was obtained by flowing the liquid sample in a cylindrical cell across the CW pump and probe beams. The two beams were focussed by lenses (L_1, f_1 = 160 mm; L_2, f_2 = 80 mm) into the cell, whose internal dimensions were 42 mm (diameter) and 5 mm (height). An image of the probe beam waist was formed on the entrance slit of the spectrometer with an enlargement factor of 4.5. The distance between the probe beam and the rotation axis of the cell was 20 mm. Its rotational frequency was varied between 10 and 50 s^{-1}, giving flow velocities (v) of 1.26 and 6.28 m s^{-1}, respectively. The pump beam was interrupted periodically ($\sim$10 s^{-1}), which enabled us to record probe-only and pump-and-probe spectra quasisimultaneously.

Detection of Raman Spectra. For excitation of Raman scattering, we used the green and blue lines of an argon laser (Coherent, Innova 70). Photoreactions of BR_{570} and its intermediates in the probe beam were kept low by choosing photoconversion parameters below 0.2. A mixture of BR_{570} and its green-absorbing intermediates L and N was probed, with the green line at 514 nm, whereas the blue line at 476 nm was used to monitor BR and its intermediates L, M, and N simultaneously. The scattered light was monitored perpendicularly to the probe beam by a conventional Raman spectrometer (Spex 14018 double monochromator, photomultiplier EMI 9659 QB). This was controlled by a microcomputer in combination with a Spex Compudrive (CD2A). The Raman signals were collected into the memory of a counter device (Ortec 874) as photon counts per second for each spectral position. Overview spectra between 700 and 1700 cm^{-1} were recorded with a step width of 1 or 2 cm^{-1}. For

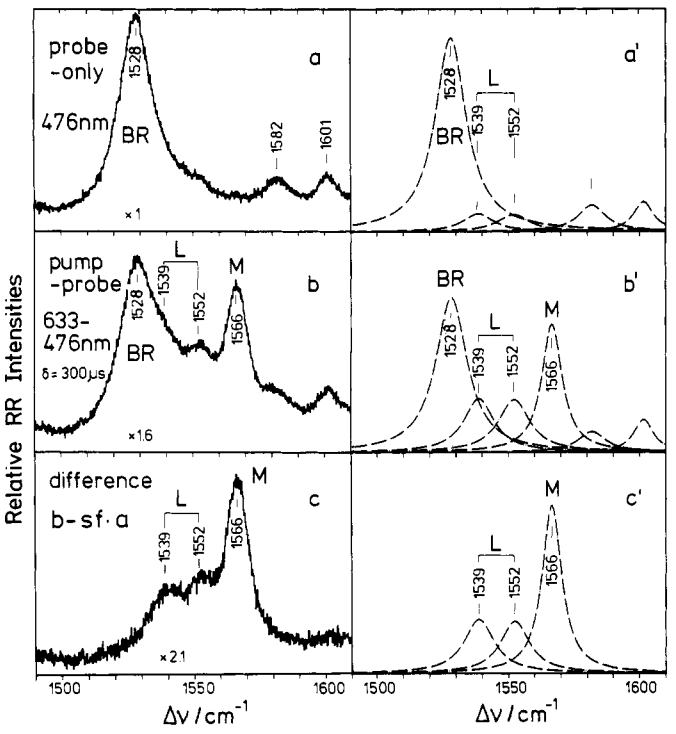

FIGURE 2: RR spectra in the C=C stretching region from an aqueous suspension of purple membranes (pH 5, 22 °C, OD = 1 at 570 nm). The spectra were obtained with a flow velocity v = 1.26 m s^{-1} using the equipment described in Figure 1. Pump beam: λ_P = 633 nm, $\overline{d_P}$ = 160 μm, and P_0 (laser power) = 80 mW. Raman probe beam: λ_R = 476 nm, $\overline{d_R}$ = 80 μm, and P_0 = 3.3 mW. The band-fitting and difference procedures are described in the text.

precise measurements in a narrow range (1490–1610 cm^{-1}), a step width of 0.2 cm^{-1} was used. In all cases, the dwell time at each spectral position was 1 s and the spectral bandwidth was ~4 cm^{-1}.

In our optical device (Figure 1), the pump beam was interrupted periodically (~10 s^{-1}) by a chopper. By coupling the chopper with two different memories in the counter device, we were able to accumulate probe-only and pump-and-probe spectra in a quasisynchronous way. The probe-only Raman signal of the parent species then can be used as an internal standard for the quantitative analysis of the spectra. Up to 100 scans were added to obtain spectra of sufficiently good quality for band-fitting analysis and difference procedures.

Analysis of the Pump-Probe Spectra. The analysis of a typical pump–probe RR experiment is illustrated in Figure 2. The conditions were chosen in a way that, besides the parent species, only the intermediates L and M made contributions to the Raman signal. The spectral records were analyzed by a least-squares band-fitting procedure with Lorentzian line shapes using spectral parameters which had been obtained in separate experiments for the individual species. From the bands in Figure 2, the "normalized RR intensities" were calculated, which are defined as the integrated intensities of the characteristic ethylenic RR bands in the pump–probe spectrum with respect to the integrated intensity of the C=C stretch of BR_{570} at 1529 cm^{-1} in the probe-only spectrum (Diller & Stockburger, 1988). The relative concentrations (in brackets) are related to the normalized RR intensities (I_{RR}) by

$$\sum_i [C_i] + [\mathrm{BR}] = \sum_i f_i(\lambda_R) I_{RR}(i) + I_{RR}(\mathrm{BR}) = 1 \quad (2)$$

where i refers to the intermediates, R refers to the Raman probe beam, and the factors $f_i(\lambda_R) = \sigma_{BR}(\lambda_R)/\sigma_i(\lambda_R)$ relate the RR scattering cross section of BR_{570} to those of the intermediates. It is evident from this definition that $I_{RR}(BR)$ is equal to the relative concentration of BR_{570} in the pump–probe spectrum.

In Figure 2c the contribution of BR_{570} was subtracted from the pump–probe spectrum. The subtraction factor (sf) is given by the relative concentration of BR_{570} in the pump–probe spectrum, i.e., by $I_{RR}(BR)$. Such "difference spectra" will be used in this paper to illustrate the time dependence of the various intermediates.

Laser Flash Photolysis Experiments. Aqueous suspensions of purple membranes (OD ≈ 1 at 570 nm, 20 °C) were photolyzed in a fluorescence cuvette (10 × 10 × 50 mm) using a frequency-doubled Q-switched Nd:YAG laser (Lumonics HY 400; 532 nm, 8-ns pulse duration). The pulse energy was attenuated to 3.7 mJ and the beam was expanded to obtain a photoconversion parameter ($\overline{I_B}\Delta t$) of 3.4. Under such conditions, OD changes of 28% at 570 nm were induced in the sample by a single laser flash.

For the probe beam the light of a tungsten lamp was dispersed by a monochromator and aligned perpendicularly to the laser beam. Probe and laser beams were centered to each other in the middle of the fluorescence cuvette, where they had diameters of 4 and 7 mm, respectively. Light adaption (i.e., all bR molecules are pumped by light into the active parent state BR_{570}) was accomplished by preillumination of the sample with more than 100 laser flashes. Both beams were linearly polarized, and the angle between their polarization vectors was set to the "magic value" of 54.7° in order to exclude the influence of orientational motion of the chromophore on the transient signals. Behind the sample, the probe beam passed through a second monochromator to discriminate the probe light from the scattered laser light. At its exit slit the transient signals were detected by photomultiplier tubes (R106 or R928 from RCA) and analyzed by a transient recorder (Le Croy 8828 C). The response time of the electronic entrance circuit was 10 μs for the measurements on the ms time scale and 60 ns for the μs time scale. The time base for the transient signal was varied between 80 and 400 ms, and 8192 (=2^{13}) data points were linearly distributed over each selected time base.

Different probe wavelengths were selected between 400 and 700 nm, and for each value the pH of the sample was varied in steps between 3 and 12. Energy fluctuations between sequential laser flashes were below 1%. Up to 500 flash-induced transient signals were averaged for each fixed value of the wavelength and the pH. The repetition rate was 0.5 s^{-1}. The transient signals were converted into absorbance changes. A sum of exponentials was used for fitting such curves, following the procedure of Provencher (1976). The residuals between the measured and calculated time courses as well as their autocorrelation functions served as criteria for the best fit. When there was no improvement while going from n to n + 1 exponentials, n was chosen as the most suitable number.

RESULTS AND DISCUSSION

Intermediates M^f and M^s. We begin with a description of the pH-dependent kinetic behavior of the intermediate M_{412}, which is important for the analysis of the photocycle. We have studied transient absorbance signals at 412 nm over the range pH 4–10. A good fit to the data for the decay of M in the entire pH range could be achieved by the superposition of two exponentials, $M^f(\tau^f)$ and $M^s(\tau^s)$ (Figure 3a). A drastic

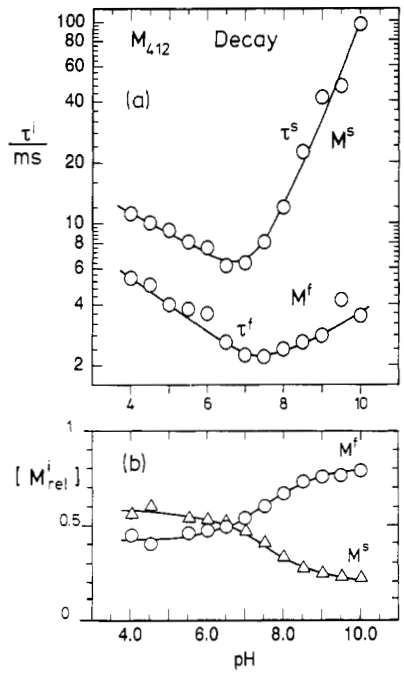

FIGURE 3: (a) The two decay constants of M, τ^s and τ^f, deduced from optical transients at 412 nm (20 °C). (b) Relative amplitudes: $M^f_{rel} = M^f/(M^f + M^s)$; $M^s_{rel} = 1 - M^f_{rel}$.

increase of τ^s is observed for pH > 7.5. This effect had been report earlier (Scherrer & Stoeckenius, 1985; Otto et al., 1989).

The pH dependence of the relative amplitudes $M^f_{rel} = M^f/(M^f + M^s)$ and $M^s_{rel} = M^s/(M^f + M^s)$ is shown in Figure 3b. It can be seen that M^f_{rel} and M^s_{rel} change significantly as a function of pH. Later it will be shown that on a calibrated scale it is mainly M^f which increases with pH (cf. Figure 16). The increase of M^f_{rel} (decrease of M^s_{rel}) with increasing pH can be described by a midpoint value of pH 7.5.

It turned out that in the range pH 4–8 the formation of M_{412}, as deduced from the transient absorbance signal at 412 nm, can be well fitted by a single time constant (τ_2). Under the conditions of Figure 3 this has a value of ~80 μs. It follows from our earlier RR experiments on the decay of L (Diller & Stockburger, 1988) that this time constant is directly correlated with the "fast" decay component of L (L_{fd}).

In agreement with the work of Hanamoto et al. (1984), we found that for pH > 8 the time constant for the formation of M decreases to ~7.5 μs. Under the conditions of Figure 3, this effect can be described by a titration-like curve with a pK_a value of 9.2.

Definition of the Intermediate N by Its Resonance Raman Spectrum. The intermediate N plays a key role in the photocycle of bR. This requires a detailed description and a precise definition. An intermediate N with a protonated Schiff base which appears as a direct product of M had already been invoked in the early work on the photocycle of bR (Lozier et al., 1975). However, this proposal was merely based on the observation that a green-absorbing species exists on the same time scale as M. Later it was found that under certain conditions (purple membrane suspension at high pH, high pH plus high salt concentration, or in detergents) a green-absorbing species adopts the longest lifetime of all intermediate states in the photocycle. This made it possible to characterize this species spectroscopically (Dancsházy et al., 1986; Drachev et al., 1987; Kouyama et al., 1988). Its formation could be correlated by Kouyama et al. (1988) with the decay of M^f, and therefore the name N was proposed.

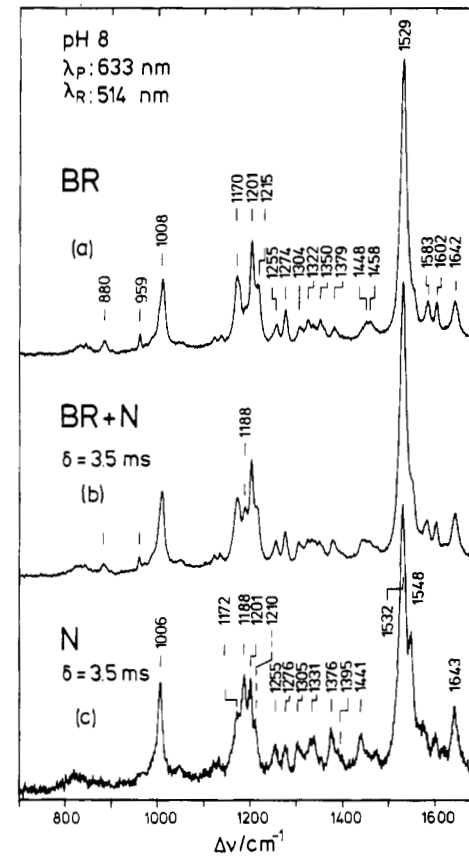

FIGURE 4: RR spectra from an aqueous suspension of purple membranes (pH 8, 22 °C, OD = 1 at 570 nm) using the equipment described in Figure 1 with a flow velocity $v = 1.26$ m s^{-1}. Pump beam: same conditions as in Figure 2. probe beam: $\lambda_R = 514$ nm, $d_P = 80$ μm, and $P_0 = 3.5$ mW. The upper probe-only spectrum represents the parent chromophore. The pump–probe spectrum in the middle, obtained with a delay time $\delta = 3.5$ ms, represents a mixture of BR_{570} and N. The lower trace reflects the pure spectrum of N obtained from the difference procedure described in the text.

In Figure 4 is shown how the RR spectrum of a green-absorbing intermediate which might be a direct product of M^f can be obtained in a pump–probe experiment as described in Materials and Methods. A delay time of 3.5 ms between pump and probe events was chosen, which is somewhat higher than τ^f (cf. Figure 3). The probe beam at 514 nm guarantees selective RR excitation in the green and thus excludes a significant contribution of M_{412}. The pure spectrum of the intermediate in Figure 4c was obtained by subtracting the probe-only spectrum in 4a to such an extent that the band at 880 cm^{-1}, which is characteristic of BR_{570}, vanishes.

The RR spectrum of the green-absorbing intermediate described by Kouyama et al. (1988) had first been obtained by Alshuth and Stockburger (1986) when they studied the photocycle at pH 9.6. It was concluded in particular from the isotope effects observed in D_2O suspension that the structure of this species must be very similar to the structure of L. It therefore was described as an L-like intermediate (cf. Figure 5d). RR spectra of this intermediate under similar conditions were also obtained by Fodor et al. (1988) and Nakagawa et al. (1991). It was reported by Diller and Stockburger (1988) that at neutral pH a similar species is formed in a fairly fast process (200–300 μs). Since no M precursor could be identified, this intermediate was assigned to a direct product of L and was therefore called L′ (Diller & Stockburger, 1988). A spectrum of this species obtained for a delay time of 600 μs is depicted in Figure 5b.

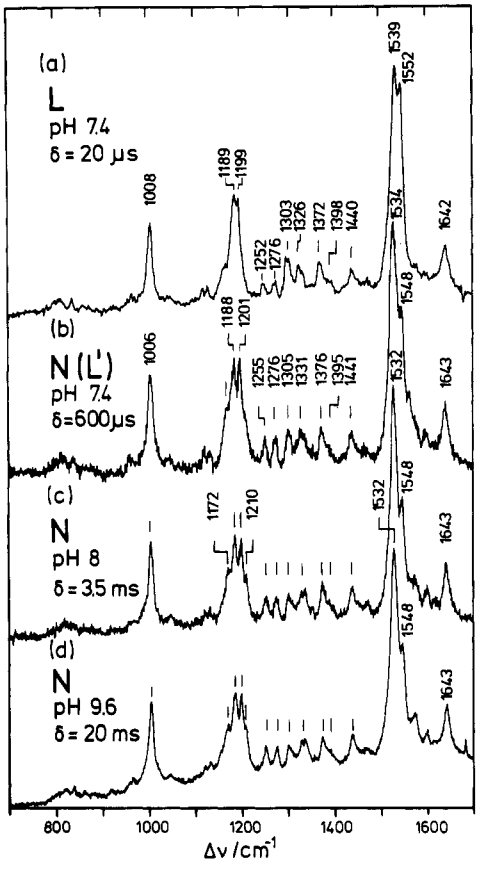

FIGURE 5: RR spectra of L and N for different pH values and delay times. All other experimental conditions are the same as given in Figure 6 for L and in Figure 4 for N.

It is thus suggested that the green-absorbing intermediate, defined by its distinct RR spectrum (Figure 5), is formed in different reaction pathways. In the present paper we adopt the name N for this intermediate. However, it must be noted that this does not mean that N necessarily is a direct product of M.

Structure of N. It turns out from Figure 5 that the spectra of N and L are very similar. Consequently, their structures must also be closely related. This is so in particular for the protonated Schiff base (Diller & Stockburger, 1988). In L, characteristic bands of this group in H_2O are the C=N stretch at 1642 cm^{-1} and a weak band at 1398 cm^{-1} which is due to an N–H in-plane bending mode. In the case of N these bands appear at 1643 and 1395 cm^{-1} (cf. Figure 5). Still more characteristic are the isotope effects of the Schiff base bands in D_2O where the nitrogen is deuterated [cf. Figure 14 in Alshuth and Stockburger (1986); there N is denoted by "L"). These effects are completely analogous in L and N. Thus, in D_2O the C=N stretch is downshifted by ~25 cm^{-1} and the bandwidth is narrowed [for an interpretation of this effect, see Hildebrandt and Stockburger (1984)]; the N–H rock at ~1395 cm^{-1} vanishes, and finally a new relatively strong band arises at 985 cm^{-1} which could be assigned to the isolated C–H out-of-plane bending mode of the Schiff base group (Stockburger et al., 1986). This analogy in all spectral details strongly suggests that the geometry and the electronic structure of the Schiff base group are the same in L and N. This allows the conclusion that the immediate environment of the Schiff base, including the negative counterion, is the same for both species. In particular this would imply that L and N have the same negative counterion to the positively charged Schiff base. There is much evidence from different types of experiments that the counterion in L is the carboxylic side chain of the residue Asp-85 (cf. below for a more detailed discussion). Consequently, in L and in N, Asp-85 would be deprotonated.

It was proposed that the 13-*cis* configuration of the retinal chain in L is preserved in N (Fodor et al., 1988). On the other hand, distinctive spectral differences occur in the C=C stretching region where the low-frequency peak in L at 1539 cm^{-1} is shifted to 1532 cm^{-1} in N. This band can be assigned to the "in-phase" C=C stretching mode (sometimes called the ethylenic mode) of the retinal chain whose frequency is extremely sensitive to π-electron delocalization (Grossjean et al., 1990). It is well established on an empirical and theoretical basis that a proportionality exists between the frequency of the ethylenic band of a bR chromophore and the λ_{max} value of its optical absorption band (Kakitani et al., 1983). Using frequencies of 1528 and 1539 cm^{-1} and λ_{max} values of 570 and 550 nm for BR_{570} and L, respectively, and a frequency of 1532 cm^{-1} for the ethylenic band of N, one obtains from a linear interpolation a value for $\lambda_{max} \approx 560$ nm for N, in good agreement with the optical data (Kouyama et al., 1988; Drachev et al., 1987).

It is of basic interest to understand the structural difference between L and N which is reflected by the downshift of the ethylenic mode from 1539 to 1532 cm^{-1}. According to the arguments above, this shift cannot be caused by structural changes in the vicinity of the Schiff base group. It has been argued by Lohrmann and Stockburger (1992) that the big upshift of the ethylenic mode from 1518 cm^{-1} in K to 1539 cm^{-1} in L is at least partially caused by an interaction of the retinal moiety with a positively charged group which approaches the retinal moiety during the K-to-L transition. In this picture the downshift of the ethylenic band when going from L to N would imply that the positive charge is again removed from the retinal moiety. It is thus obvious from the RR spectra that it is the environment of the retinal moiety which has changed in N compared to L.

Protein Backbone Conformation in L and N. The N state could also be identified by difference Fourier transform infrared (FTIR) spectroscopy (Pfefferlé et al., 1991; Braiman et al., 1991; Ormos et al., 1992). This technique reveals not only the light-induced changes of the chromophore but also conformational changes of the polypeptide chain. It was found by Ormos (1991) that, as a function of temperature, the protein backbone undergoes a sharp conformational transition at ~250 K which later was correlated with the M-to-N transition (Braiman et al., 1991; Ormos et al., 1992). However, it turned out that in the site-specific mutant D212N (Asp-212 is replaced by Asn), in which M is not found, the intermediate N appears as a direct product of L, simultaneously with the protein conformational transition, with a time constant of ~220 μs at 20 °C and pH 8 (Cao et al., 1993). It was therefore concluded that the de- and reprotonation of the Schiff base is not a prerequisite for the formation of N, but that this event is associated with the observed conformational transition of the protein backbone.

If one denotes the protein states in L and N by P(L) and P(N), the only condition for the observation of N in the photocycle then would be that the transition P(L) → P(N) takes place. Since P(N) can be formed also when the Schiff base remains protonated, one expects a direct L → N transition in the photocycle of wild-type bR. Such a transition was reported by Diller and Stockburger (1988). Since, on the other hand, the reaction sequence L → M → N is also observed in the photocycle, it appears that the protein state P(N) can also be formed when the chromophore is in the M state.

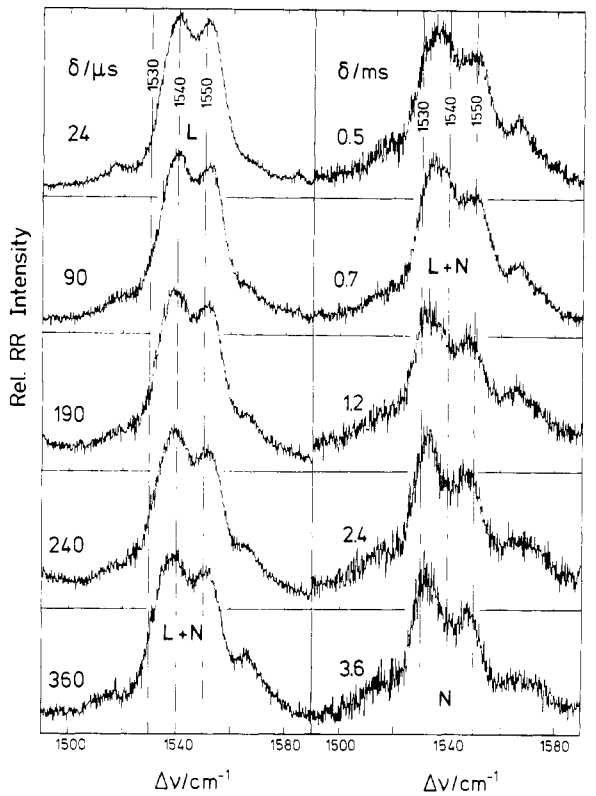

FIGURE 6: RR spectra of L and N (pH 7.4, 22 °C) in the C=C stretching region from a pump-and-probe flow experiment (v = 6.28 m s^{-1}) with delay times between 24 μs and 3.6 ms. Pump beam: λ_P = 647 nm, d_P = 160 μm, and P_0(laser power) = 350 mW. Raman probe beam: λ_R = 514 nm, d_R = 60 μm, and P_0 = 5 mW. The difference procedure is the same as in Figure 2.

Formation of N, Probed at 514 nm (pH 7.4). The spectra in Figure 6 display the region of the characteristic C=C stretching vibrations. Under such conditions the spectra are mainly composed of bands of the green-absorbing intermediates L and N, whereas the blue-absorbing M_{412} does not contribute significantly. The spectrum at a delay time of 24 μs is due exclusively to L, which is characterized by its two peaks of equal intensity at 1539 and 1552 cm^{-1}. On the other hand, the spectra for $\delta > 1$ ms can be exclusively attributed to N according to its characteristic peaks at 1532 and 1548 cm^{-1} of unequal intensity. Starting from the low limit δ = 24 μs, the contribution of L decreases, whereas that of N rises, with increasing delay time. This allows the conclusion that the formation of N in the time domain up to ~1 ms is correlated with a "slow-decaying" L component.

This behavior is further elucidated by a quantitative evaluation of the data as given in Figure 7. In this procedure the normalized RR intensities of the sum L + N were obtained from the respective double peaks of the two species in the C=C stretching region. Then the relative contributions of L and N were inferred from the composite spectra. For this purpose a calibration curve was constructed from the pure spectra of L and N which correlates the position of the low-frequency peak in the composite spectra with the relative contributions of the two species. The time dependence of the RR intensity of N obtained in this way is given in Figure 7 by triangles, whereas the slow decay of the RR intensity of L (L_{sd}) is indicated by the dashed curve. From this curve one deduces an exponential decay time of ~360 μs for L_{sd}.

It has been proposed that N is a direct product of M^f (Kouyama et al., 1988; Fodor et al., 1988). One would therefore expect that N has a rise time of ~2 ms (cf. Figure 3a). However, it is evident that under the conditions of Figure 7 the rise of N is dominated by a component which is considerably faster. This "fast-rise component", N_{fr}, is correlated with the slow-decaying L component (L_{sd}). For its reaction sequence one obtains

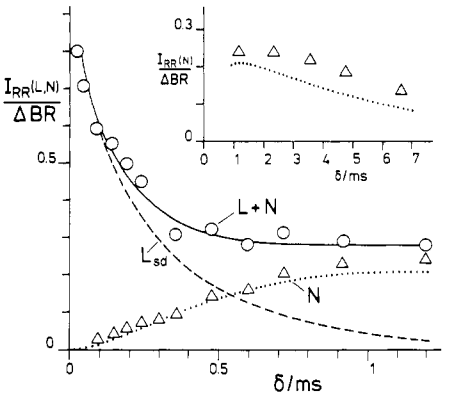

FIGURE 7: Time dependence of the RR intensity of the C=C stretching bands of L and N from experiments performed as described in Figure 6. The fractional contribution of N to the total RR intensity, L + N, is given in good approximation by $\Delta\nu/\Delta\nu_{max}$, where $\Delta\nu$ is the downshift of the low-frequency peak in the spectra of Figure 6 and $\Delta\nu_{max}$ = 7 cm^{-1} refers to the shift of the low-frequency C=C stretch when going from L (1539 cm^{-1}) to N (1532 cm^{-1}). A somewhat different procedure is described in the text.

$$\cdots L_{sd} \xrightarrow{\tau_{fr}} N_{fr} \xrightarrow{\tau_N} BR_{570} \qquad (3)$$

The dotted line in Figure 7 shows the time dependence of N_{fr} according to eq 3 using τ_{fr} = 0.5 ms and τ_N = 6 ms. For δ < 0.6 ms there is good agreement with the experimental data. The deviations at longer delay times indicate that a second slow-rising N component is involved.

It must be noted that our data do not allow the definite exclusion of an intermediate M in eq 3. Following the decay of L_{sd}, this M component should have a rise time of 360 μs. In order to fit the formation of N_{fr} (dotted line in Figure 7), its decay time should be 170 μs. It can be estimated that the maximum concentration of this M component in the photocycle would be only ~10% of the total amount of M and therefore would be hard to identify experimentally. In the following such an intermediate M component will not be further considered.

Formation of N, Probed at 476 nm (pH 7.6). Additional insight into the formation process of N can be obtained from RR spectra excited at 476 nm. At this wavelength RR scattering from M is of similar strength as from L, N, and BR_{570} so that the fractional concentrations of these four species can be monitored in the same experiment. In Figure 8a a series of spectra (at pH 7.6) over the time range 0.4–3.6 ms is displayed for the region of the characteristic C=C stretching bands. The various records were normalized to equal height of the peak at 1566 cm^{-1}, which represents the ethylenic band of M. Since the fast decay of L occurs with a time constant of ~80 μs, this component is completely converted to M already for the shortest delay time of 0.4 ms. On the other hand, the slow-decaying L component can still be identified at 0.4 ms. With increasing values of δ this component is converted to N.

The fractional concentrations of BR_{570} and its intermediates were obtained as described in Materials and Methods. According to Figure 14, the maximum accumulation of the intermediate O at pH 7.6 is only ~5% of ΔBR (in this paper the notation "ΔBR" is used for the fraction of bR which is

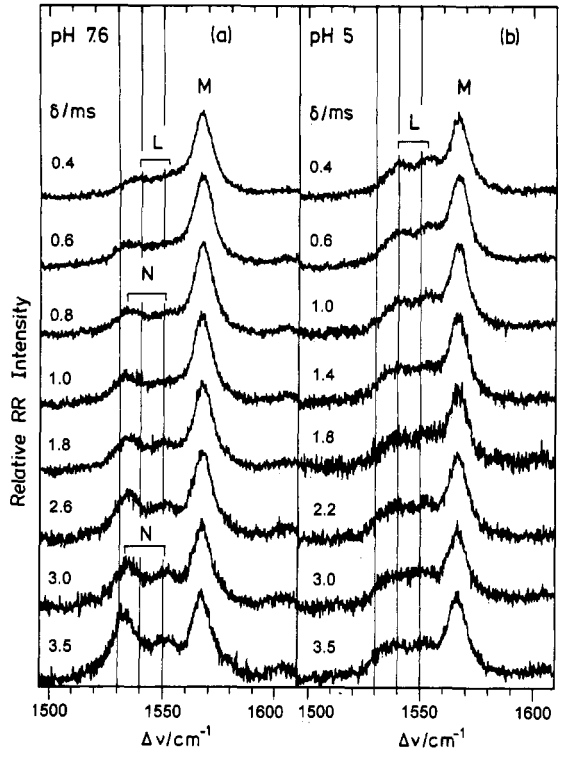

FIGURE 8: RR bands of L, M, and N in the C=C stretching region for delay times in the range 0.4–3.5 ms: (a) pH 7.6; (b) pH 5. Other experimental conditions were the same as in Figure 2.

converted to intermediates in the photolysis beam). Therefore, the contribution of O will be neglected in the following consideration. In this approximation one obtains from eq 2 for the sum of the fractional concentrations

$$f_L I_{RR}(L) + f_M I_{RR}(M) + f_N I_{RR}(N) + I_{RR}(BR) = 1 \quad (4)$$

The factors f_i for the probe wavelength 476 nm were determined on the basis of eq 4. Thus $f_L \approx 1$ was inferred from mixtures which contain nearly equal amounts of BR_{570} and L but only a small fraction of M. $f_M = 1 \pm 0.1$ was inferred from the data in Figure 13a,b which contain contributions from BR_{570}, L, and M. Finally $f_N = 1.5 \pm 0.1$ was obtained from our set of data in Figure 9, which contains a significant contribution of N. The normalized RR intensities $I_{RR}(i)$ were deduced from the integrated intensities of the strong C=C stretching bands: BR_{570} (1528 cm^{-1}), L (1539 + 1552 cm^{-1}), M (1566 cm^{-1}), and N (1532 + 1548 cm^{-1}).

The results are displayed in Figure 9. The error limits of the data points essentially depend on the accuracy by which the C=C stretching bands of the various species could be separated by band-fitting and difference procedures. Evidently, this accuracy strongly depends on the quality of the original RR spectra. Depending on the amplitude of the bands, the standard deviation lies between 10 and 20%. However, the quality of the data is demonstrated independently by the good agreement of the time-dependence of $M^f + M^s$ obtained from the RR experiments (triangles) and from our optical transient studies under identical conditions (dotted line).

For understanding the time dependence of ΣN in Figure 9 in addition to N_{fr} in eq 3, a "slow-rise component", N_{sr}, has to be considered according to

$$\cdots L_{fd} \xrightarrow[80\mu s]{\tau_2} M^f \xrightarrow[2ms]{\tau^f} N_{sr} \xrightarrow[6ms]{\tau_N} BR_{570} \quad (5)$$

where L_{fd} refers to a fast-decaying L component, and the

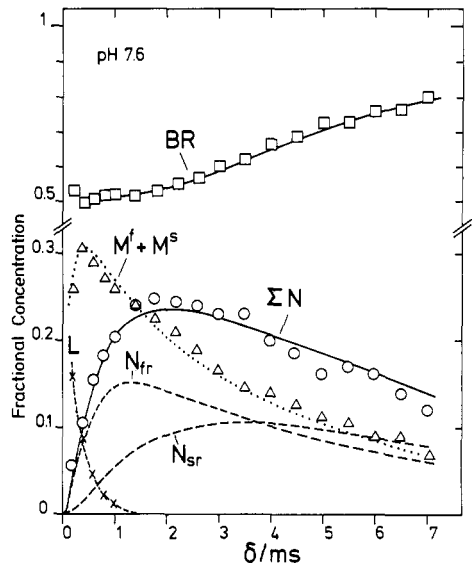

FIGURE 9: Fractional concentrations of L, M, and N in the time range 0.2–7 ms at pH 7.6. Up to δ = 3.5 ms the experimental conditions were the same as in Figure 2. For $\delta \geq 3.5$ ms the conditions for the pump beam were modified: λ_P = 647 nm, $\bar{d}_P$ = 500 μm, and P_0 = 500 mW. The decomposition of the total RR intensity in the C=C stretching region reveals the components N_{fr}, N_{sr}, and L. In analogy to eq 3, N_{fr} was calculated as a direct product of L_{sd} using τ_{fr} = 0.5 ms and τ_N = 6 ms. N_{sr} was calculated according to eq 5. The initial amplitudes of L_{sd} and L_{fd} were chosen to fit the measured total RR intensity. The dotted line displays the decay of M obtained by optical transient studies at 412 nm for an identical sample of PM.

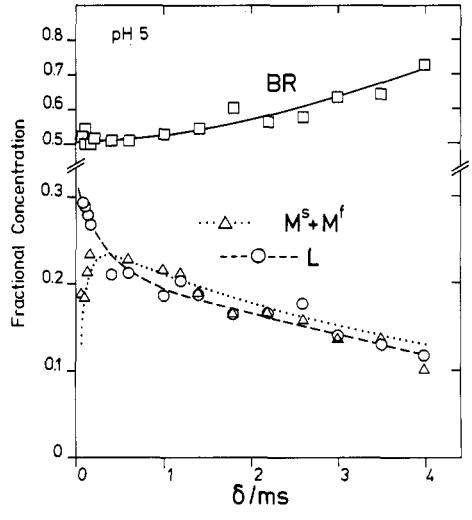

FIGURE 10: Fractional concentrations of L, M, and N at pH 5. Other conditions are as in Figure 9.

given time constants refer to the conditions in Figure 9. A good fit to ΣN in Figure 9 is obtained by a superposition of N_{sr} and N_{fr} in eqs 3 and 5 with equal initial values of L_{sd} and L_{fd} (see also the caption to Figure 9).

Formation of N Depends on pH. A comparison of the two series of spectra in Figure 8 reveals that at pH 5 and for $\delta <$ 2 ms the intermediate N is not accumulated to a detectable level. A quantitative evaluation is given in Figure 10. Like in the case of pH 7.6, also at pH 5 can two L components be distinguished. Again, the fast decay occurs with a time constant $\tau_2 \approx 80$ μs and is correlated with the rise of M. This correspondence can be seen more clearly in Figure 10 of Diller and Stockburger (1988). However, the decay of the slow L component is delayed to several milliseconds. Only for $\delta >$

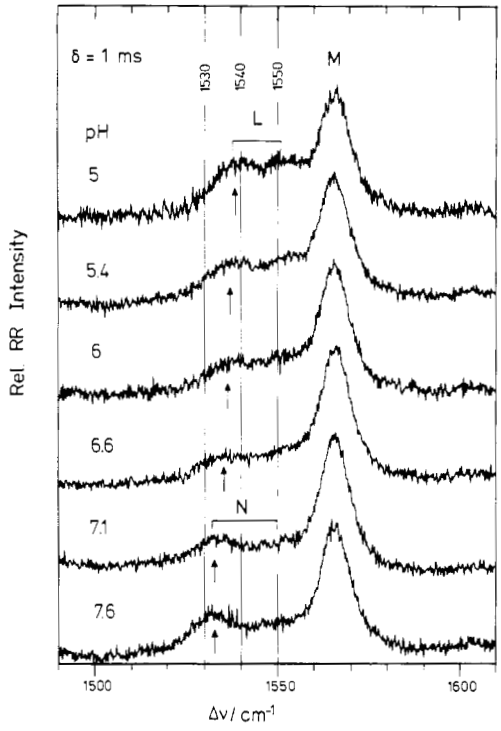

FIGURE 11: RR spectra in the C=C stretching region obtained from a pump-and-probe flow experiment for different pH values and a fixed delay time of 1 ms. All other experimental conditions were the same as in Figure 2.

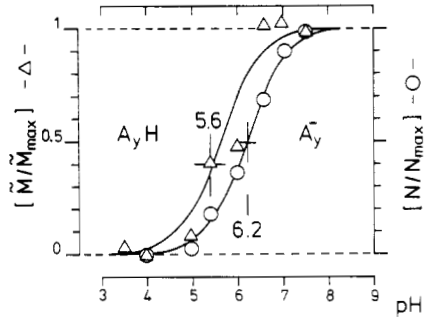

FIGURE 12: N/N_{max} is given in good approximation by $\Delta\nu/\Delta\nu_{max}$ where $\Delta\nu$ is the downshift of the low-frequency peaks (indicated by arrows in the spectra of Figure 11) with respect to the C=C stretch of L at 1539 cm^{-1}. $\Delta\nu_{max}$ = 7 cm^{-1} is the shift of the low-frequency C=C stretch when going from L to N. The pH dependence of N/N_{max} can be fitted well by a titration-like curve with pK_a = 6.2, if N is correlated with the ionized form, A_y^-, of an acidic group, A_yH, according to $N/N_{max} = [A_y^-]/([A_y^-] + [AH])$. The increment $\tilde{M}/\tilde{M}_{max}$ is deduced from the data in Figure 13 as a function of pH. A good fit is obtained by a titration-like curve with a pK_a = 5.6, if $\tilde{M}$ is correlated with the ionized form, A_y^-, of an acidic residue, A_yH, according to $\tilde{M}/\tilde{M}_{max} = [A_y^-]/([A_y^-] + [A_yH])$.

2 ms does a downshift of the band at 1539 cm^{-1} indicate the onset of the $L_{sd} \rightarrow N$ transition (Figure 8b).

The acceleration of this transition in the range pH 5–7.6 can be concluded from the series of spectra in Figure 11 obtained for δ = 1 ms. In this presentation the decay of L_{sd} and the formation of N_{fr} can be deduced from the shift of the peak at 1539 cm^{-1} (pure L) to 1532 cm^{-1} (pure N) as indicated by the arrows. On this basis the formation of N_{fr} can be displayed by the titration-like function in Figure 12. This suggests that the formation of N_{fr} is supported by the deprotonated state A_y^- of an internal A_yH group of the protein backbone whose pK_a is ~6.2. It also means that the presence of A_y^- accelerates the protein transition P(L) → P(N) in the L_{sd} state of the chromophore. It is proposed that the

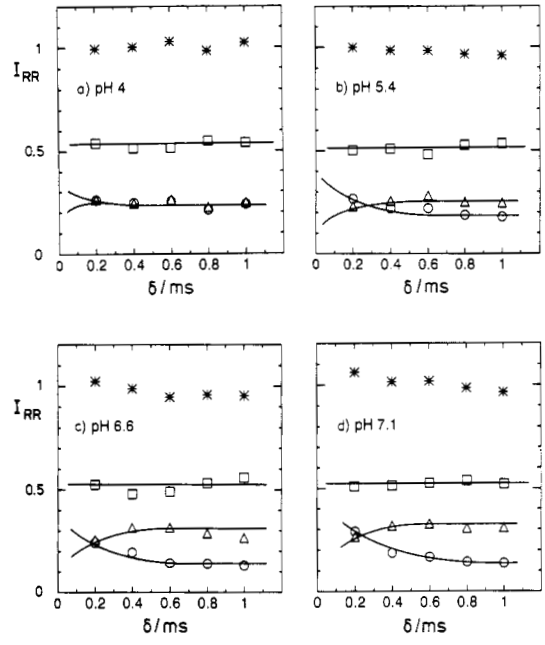

FIGURE 13: Normalized RR intensities (I_{RR}) of BR, L, M, and N + L as a function of time for different pH values. The data were deduced from experiments described in Figure 2. Panels a–d: ΣI_{RR} (*), BR (□), M (△). (○) L (panels a and b) or L + N (panels c and d).

dissociation equilibrium ($A_yH \rightleftharpoons A_y^- + H^+$) is established already in the ground state of bR. Below it will be shown that the slow-rising N component (N_{sr}) also depends on pH (cf. eqs 18 and 19).

The Increment $\tilde{M}$. In Figure 13 normalized RR intensities, probed at 476 nm, are displayed for pH values between 4 and 7.1 in the time domain 0.2–1 ms. Since for 476 nm $f_L \approx f_M \approx 1$, these quantities directly give the fractional concentrations $[BR_{570}]$, [L], and [M]. It can be seen that in this pH range the maximum of [M] increases from ~50% to ~65% of ΔBR at the expense of the slow L component (In Figure 13 ΔBR is given by $(1 - I_{RR}(BR))$ for low values of δ for which the reconstitution of BR_{570} is negligibly small). This increment of M will be called $\tilde{M}$.

If $[\tilde{M}/\tilde{M}_{max}]$ is displayed as a function of pH, one again obtains a titration-like curve which can be associated with the dissociation of a single proton from an internal group of the protein backbone. Its apparent pK_a value lies at ~5.6 (Figure 12). This behavior suggests that the formation of $\tilde{M}$ is controlled by the deprotonated form of this group. It had been demonstrated in our earlier work by a specially designed "difference experiment" [Figure 11 in Diller and Stockburger (1988)] that the increment $\tilde{M}$ can already be identified for δ = 20 μs. Since, on the other hand, the rise time of M (τ_2) is unchanged in the range pH 4–7, we conclude that the time constant for the formation of $\tilde{M}$ is close to τ_2 (~80 μs).

It thus turns out that the slow L component, observed at pH 5, is converted with increasing pH to N_{fr} or to $\tilde{M}$, respectively. Both reaction pathways appear to be controlled by the dissociated states of internal groups. The fact that the respective pK_a values are of comparable magnitude (Figure 12) suggests that the same internal group, A_yH, might be operating in both cases. It must be noted that in the model described below the two different reaction pathways will be correlated with two different species of bR so that A_yH may have somewhat different pK_a values in the two reaction pathways as is found experimentally.

Different Species of bR. The identification of kinetically different components of L can be explained by the existence

of different subspecies of bR which undergo independent cyclic reactions. Later, experiments will be described which support the validity of this concept or exclude other models.

In the following the classification of subspecies will be started with the kinetic behavior of L at pH 5. Under such conditions the manifold of bR molecules can be divided into two classes, bR(α) and bR(β), according to their ability to form M or not. According to this definition, the fractional concentration [bR(α)] is proportional of [M_{max}] in Figure 10. One obtains

$$[bR(\alpha)] = f(k_i)[M_{max}]/\Delta BR \quad (6)$$

where $f(k_i)$ is a function of rate constants. Taking into account that [M_{max}] is essentially determined by the rate constants for the rise (k_r) and decay (k_d) of M according to the linear sequence bR(α) → M → P (products), one obtains $f(k_i) = \exp[k_d/(k_d - k_r)\ \ln\ (k_d/k_r)]$ (Sherman et al., 1979). Since under the conditions of Figure 10 $k_r = (\tau_2)^{-1} \approx (80\ \mu s)^{-1}$ and $k_d \approx (6\ ms)^{-1}$, a value of 1.06 is calculated for $f(k_i)$. With $\Delta BR = (1 - [BR]_{min}) \approx 0.5$ and $[M_{max}] = 0.23$ from Figure 10 one finally obtains $[bR(\alpha)] \approx 0.5$. Then from the definition $[bR(\alpha)] + [bR(\beta)] = 1$ a value $[bR(\beta)] \approx 0.5$ is inferred. The same result can also be obtained when L in Figure 10 is decomposed into its two components, and bR(β) is inferred from the maximum of the slow L intermediate.

The two classes bR(α) and bR(β) can further be subdivided according to their kinetic behavior as a function of pH. For bR(β) one obtains from the above described evolution of the millisecond L component the two subspecies bR(β,1) and bR(β,2).

bR(β,1)

$$\text{pH 5: } \cdots\cdots L \overset{>2\ ms}{\cdots\cdots} (N) \cdots\cdots BR \quad (7)$$

$pK_a \approx 6.2$

$$\text{pH 7.6: } \cdots\cdots L \overset{\sim 0.5\ ms}{\rightarrow} N_{fr} \overset{\tau_N}{\cdots\cdots} BR \quad (8)$$

bR(β,2)

$$\text{pH 5: } \cdots\cdots L \overset{>2\ ms}{\cdots\cdots} (N) \cdots\cdots BR \quad (9)$$

$pK_a \approx 5.6$

$$\text{pH 7.6: } \cdots\cdots L \overset{\tau_2}{\rightarrow} \tilde{M}^f \overset{\tau^f}{\rightarrow} N_{sr} \overset{\tau_N}{\cdots\cdots} BR \quad (10)$$

In the reaction pathways of bR(β,2) it is assumed that $\tilde{M}$ belongs to the M^f family and therefore decays with time constant τ^f to N_{sr} in analogy to the scheme in eq 5. Direct evidence for this assignment is provided by the data in Figure 15, which will be discussed below.

The fractional concentration [bR(β,2)] can be inferred from the relation $[bR(\beta,2)] \approx [\tilde{M}]/\Delta BR$. From the data in Figure 13 one obtains $[bR(\beta,2)] \approx 15\%$ (see The Increment $\tilde{M}$ above). This gives a value of ≈35% for [bR(β,1)].

A division of bR(α) into subspecies is suggested on the basis of the two components M^f and M^s. Since M^f_{rel} and M^s_{rel} change significantly with pH (Figure 3b), such a classification must be specified for a certain pH range. At the lower pH limit the two M components approach a constant level, and this will be used to define two subspecies according to

$$[bR(\alpha,1)] = [M^s_{rel}]_{pH5}[bR(\alpha)] = 0.3$$

$$[bR(\alpha,2)] = [M^f_{rel}]_{pH5}[bR(\alpha)] = 0.2 \quad (11)$$

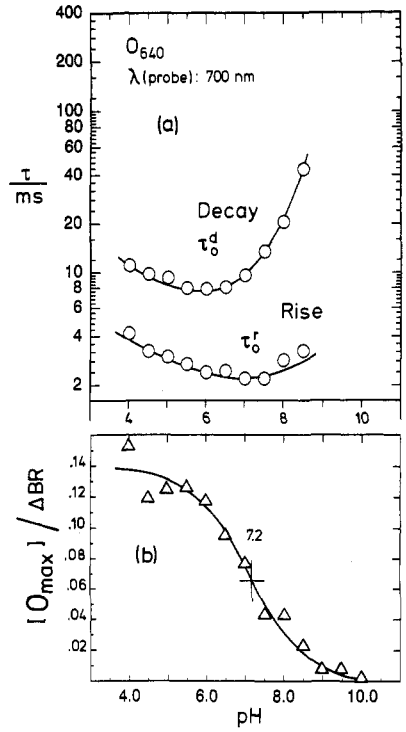

FIGURE 14: Rise and decay times of O_{640} as functions of pH probed at 700 nm by optical transient measurements (20 °C). In the lower part $[O_{max}]/\Delta BR$, defined in the text, is displayed as a function of pH.

The related photocycles can be described by

$$\text{pH 5, bR}(\alpha,1): \cdots\cdots L \overset{\tau_2}{\rightarrow} M^s \overset{\tau^s}{\cdots\cdots} (M^*) \cdots\cdots BR \quad (12)$$

$$\text{pH 5, bR}(\alpha,2): \cdots\cdots L \overset{\tau_2}{\rightarrow} M^f \overset{\tau^f}{\rightarrow} (O) \cdots\cdots BR \quad (13)$$

Later it will be shown that in the cycle of bR(α,2) the intermediate O_{640} is formed. It will further be argued that in the cycle of bR(α,1) only a short-lived M intermediate (M*), which, however, is not accumulated, appears between M^s and BR_{570}. It will be demonstrated that the two cycles change drastically with increasing pH.

The Intermediate O_{640}. It is well established that in the transient spectra of bR positive absorbance changes arise between 620 and 700 nm with time constants of 2–3 ms. They were attributed to an intermediate called O_{640} which was thought to be a direct product of N (Lozier et al., 1975; Kouyama et al., 1988). In Figure 14a the time constants for the rise and decay of the 700-nm absorbance are given in the range pH 4–10. Figure 14b shows the maximum value of the fractional concentration of O (with reference to ΔBR) as a function of pH, inferred from the optical transients at λ_r = 660 and 700 nm. This quantity can be calculated from the peak heights of the negative (ΔOD^-) and positive (ΔOD^+) loops in the optical transients which reflect the bleaching of BR_{570} (ΔBR) and the subsequent formation of O. After excitation, these peaks appear with delays of ~0.4 and ~3 ms, respectively. One obtains

$$[O_{max}]/\Delta BR = \left[\frac{\Delta OD^+}{\Delta OD^-}\frac{\epsilon(BR)}{\epsilon(O)}\right]_{\lambda_r} \quad (14)$$

Reference was made to ΔOD^- at pH 4 in order to avoid errors caused by pH-dependent effects on the bleaching of BR_{570}. Equation 14 was evaluated for λ_r = 660 nm using a value of

$\epsilon(O)/\epsilon(BR) = 16$ at 660 nm, which was inferred from Figure 3 of Váró et al. (1990). Since at $\lambda_r = 700$ nm no reliable values for $\epsilon(O)/\epsilon(BR)$ are available, the data were normalized to $[O_{max}]/\Delta BR$ (pH 4–5) at $\lambda_r = 660$ nm. In Figure 14b only values for $\lambda_r = 700$ nm are given, since for pH > 7 the ΔOD^+ signals at 660 nm are perturbed by contributions from the decay of N to BR_{570}. The decrease of $[O_{max}]/\Delta BR$ in the pH range 6.5–8.5 can be associated with a midpoint value of 7.2. The strong pH dependence of O had also been reported earlier (Li et al., 1984, and references therein).

In the recent literature the O intermediate was assigned by most authors to a direct product of N (Kouyama et al., 1988; Chernavskii et al., 1989; Ames & Mathies, 1990; Váró et al., 1990; Chizhov et al., 1991). This assignment, however, is difficult to reconcile with the pH dependence of N and O, which goes in the opposite direction (cf. Figures 12 and 14). If N were a direct precursor of O, its decay time should match the rise time of O. At neutral pH and room temperature N has a lifetime of ~6 ms (Figure 9), whereas the rise time of O is ~2.5 ms (Figure 14).

From our data it is rather suggested that O is a direct product of M^f. Thus, it can be inferred from Figures 3a and 14a that in the range pH 4–6, where O obtains its highest concentration, the rise time of O directly matches the decay time of M^f. On the other hand, in the range pH 4–6 the decay of O matches the recovery time of BR (cf. Figures 14a and 15a). This behavior is consistent with a reaction sequence $M^f \rightarrow O \rightarrow BR_{570}$, which had already been proposed earlier (Sherman et al., 1979).

A characteristic feature of O is its pH dependence, which can be described by a titration-like function with a pK_a of ~7.2 (Figure 14b). If this is associated with the acid–base equilibrium of a distinct internal group (A_uH), the negative slope of the curve indicates that the existence of the protonated form is a prerequisite for the formation of O. This is just the opposite behavior of that we had found for the formation of N_{fr} and $\tilde{M}$.

The peculiar pH dependence of O suggests that this intermediate occurs in the photocycle of a subspecies of bR. In the range of pH 4–6, where O has its maximum concentration, the only M^f component occurs in the photocycle of bR(α,2) in eq 13. This M^f component therefore can be considered as the precursor of O, so that eq 13 can now be written in the form

$$\underline{bR(\alpha,2)},\ pH < 7.2:\ \cdots\cdots L \xrightarrow{\tau_2} M^f \xrightarrow[\tau_O^f]{\tau^f} O \xrightarrow{\tau_O^d} \cdots\cdots BR \qquad (15)$$

There is no doubt that O has a protonated Schiff base. If one accepts that O is in all-*trans* configuration (Smith et al., 1983), the transition from M^f to O involves both the reprotonation of the Schiff base and the reisomerization of the retinal chain. Later it will be argued that the formation of O requires the participation of two internal protons. The internal group A_uH in its acidic form may act as a donor for one of the protons or may mediate this process indirectly.

When A_uH is deprotonated already in the unphotolyzed species according to a pK_a of 7.2, one proton must be taken up from the external phase so that for pH > 7.2 the decay of M to O would be significantly delayed. We therefore correlate for pH > 7.2 the M^s component whose lifetime strongly increases with pH in the alkaline region (cf. Figure 3) with bR(α,2). This gives

$$bR(\alpha,2),\ pH > 7.2:\ \cdots\cdots L \xrightarrow{\tau_2} M^s \overset{[H^+]}{\underset{\tau^s}{\cdots\cdots}} (O) \cdots\cdots BR \qquad (16)$$

In this reaction the formation of O would be significantly delayed for pH > 7.2. Since, on the other hand, the conversion of O to BR_{570} should be independent of pH, the intermediate concentration of O in eq 16 would decrease for pH > 7.2 in agreement with experimental evidence.

An independent criterion for the validity of the assignments in eqs 15 and 16 would be that the fractional concentration of 0.2 for bR(α,2) in the original definition of eq 11 is consistent with the reactions in eqs 15 and 16. In the case of eq 15 a value of $[bR(\alpha,2)]$ can be inferred from $[O_{max}]/\Delta BR$ (Figure 14b) and the various rate constants of this reaction. In close analogy to eq 6, one obtains for pH 5 with $\tau_2 = 80$ μs, $\tau^f = 3$ ms, and $\tau_O^d = 8.4$ ms a value of 0.23 in good agreement with eq 11. In the case of eq 16, $[bR(\alpha,2)]$ is equal to the fraction of bR which reacts through M^s in the high-pH limit (pH 10). In this limit M is accumulated in all reaction channels (cf. Figure 16). One therefore obtains

$$[bR(\alpha,2)] = [M^s(M^s + M^f)^{-1}]_{pH10}[\sum bR(i)] \qquad (17)$$

The first factor on the right-hand side is identical with M^s_{rel} in Figure 3b, and the second one is unity by definition. This gives $[bR(\alpha,2)] \approx 0.2$ in agreement with eq 11. These results confirm the proposed assignment of bR(α,2) to the reactions in eqs 15 and 16.

Photocycles of bR(α,1). The M^s component was correlated at low pH with bR(α,1) (eq 12) but in the high-pH limit with bR(α,2) (eq 16). This means that with increasing pH M^s disappears in the photocycle of bR(α,1). The fact that the relative amplitude of M^f increases as a function of pH with a midpoint value at pH 7.5 (Figure 3b) suggests that in the high-pH limit M^f has replaced M^s in the photocycle of bR-(α,1). On the other hand, we found in our experiments at pH 7.6 that M^f is a precursor of the slow-rising N component (N_{sr} in Figure 9 and eq 5). This suggests the following description for the photocycle of bR(α,1):

<u>bR(α,1)</u>

$$pH < 7.5:\ \cdots\cdots L \xrightarrow{\tau_2} M^s \overset{\tau^s}{\cdots\cdots} BR \qquad (18)$$

$$pH > 7.5:\ \cdots\cdots L \xrightarrow{\tau_2} M^f \xrightarrow{\tau^f} N_{sr} \overset{\tau_N}{\cdots\cdots} BR \qquad (19)$$

Again it appears that the change in the cyclic reaction of a certain species, in this case the formation of the intermediate N, is controlled by the protonation state of an internal group. The various cyclic reactions which were proposed in the preceding discussion are summarized in a complete reaction scheme (Scheme I). More details will be discussed in the following section.

COMPLETE REACTION SCHEME

In the preceding analysis four different subspecies of bR could be distinguished on the basis of their specific cyclic reactions as well as by titration effects with different apparent pK_a values. It is tempting to correlate these pK_a values with single dissociable groups which control the reactions in the various subspecies. However, cooperative or surface effects cannot be excluded. No attempt will be made in this paper

Scheme I: Complete Reaction Scheme[a]

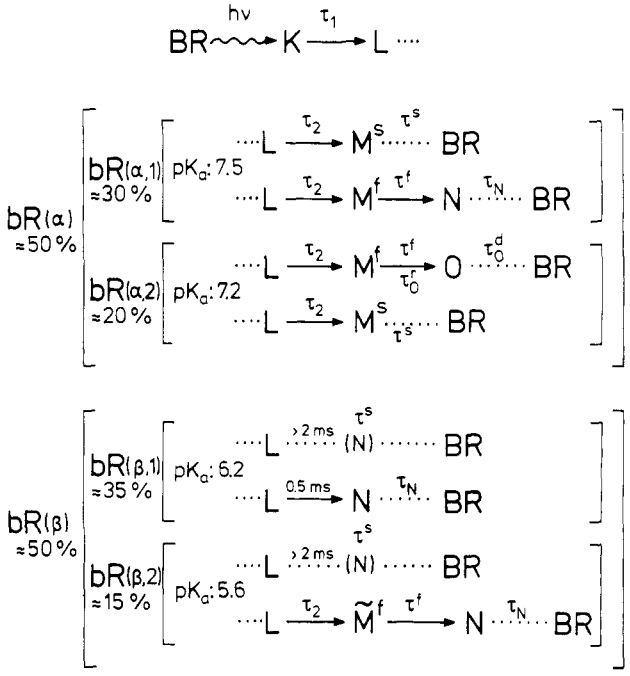

[a] τ_1 (20 °C): 1.2 μs (pH < 9), 0.8 μs (pH > 9). τ_2 (20 °C): 80 μs (pH < 9), < 7 μs (pH > 9).

to identify such groups. The fact that the various titration effects only concern fractions of bR is in favor of the heterogeneous concept. In this picture each of the related subspecies has a slightly different structure in the unphotolyzed state.

It is suggested that the different structural features we are speaking of have a fairly localized character (e.g, different conformations and environments of side chains) but do not change the overall structure of bR. In this context it is important to note that RR spectra of the parent chromophore BR_{570} remain unchanged over the range pH 4–10.5. This means that for all bR species defined in Scheme I the geometry of BR_{570} and the environmental influences on its π-electron system are the same. This implies that the structural inhomogeneities which control the different kinetic behavior must be located at some distance from the chromophore. The classification of bR in Scheme I was based on the kinetic behavior at pH 5. This procedure is arbitrary. For instance, another useful classification would be to collect all reactions with N intermediates into a single class. However, the reaction system in Scheme I is invariant to any type of classification.

In the following, Scheme I will be tested in the light of additional experimental data. Then we will ask whether other models might also explain the observed phenomena.

Optical Transients Monitored in the Range 550–600 nm. In the region of strong absorption of BR_{570} a negative absorbance change is observed which peaks ~300 μs after the excitation pulse. This negative signal is due to the bleaching of the chromophore in the reaction sequence $BR_{570} \rightarrow L_{550} \rightarrow M_{412}$. The main bleaching effect is caused by the fast decay of L to M (~80 μs). The decay of the negative signal is due to the conversion of M to products accompanied by positive absorbance changes. The essential contributions therefore are expected for M-to-BR_{570} and M-to-N transitions.

In Figure 15 the time constants and amplitudes for the decay of the negative signal, monitored at 580 and 600 nm, are displayed in the range pH 4–10. The time constant τ^s in Figure 15a which reflects the recovery of BR_{570} matches the

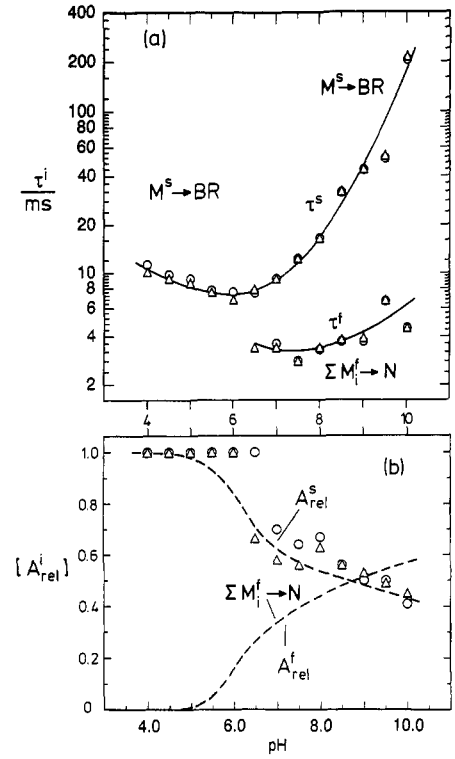

FIGURE 15: (a) Recovery times of BR, τ^s, and τ^f, deduced from optical transients at 580 nm (○) and 600 nm (△) (20 °C). (b) Relative amplitudes of $A^s_{rel} = A^s/(A^s + A^f)$; $A^f_{rel} = 1 - A^s_{rel}$.

decay time of M^s in Figure 3a over the entire pH range. This allows the conclusion that in all photocycles which involve M^s no intermediate state is significantly accumulated between M^s and BR_{570}. Later it will be shown, however, that there exists a short-lived intermediate (M*) between the two species (cf. eqs 31 and 32). The time constants τ^f in Figure 15a only slightly change with pH and are in good agreement with τ^f for the decay of M^f (Figure 3a). The relative amplitudes of the τ^s and τ^f components are displayed in Figure 15b. The fact that for pH < 6 no fast component could be identified indicates that the M^f-to-O transition (eq 15, Figure 14b) is not detectable at 580–600 nm. Moreover, since the formation of N_{fr} from L_{sd} does not lead to a negative bleaching signal, the amplitude A^f_{rel} can be exclusively attributed to the transition from M^f to N.

The data points in Figure 15b would give a step function for the relative amplitudes around pH 6.5. This, however, is not realistic. It rather reflects the limits of the analysis procedure, which does not allow us to identify the small amplitudes of the fast component below pH 6.5. In spite of such uncertainties, it is evident from the rise of the amplitude A^f_{rel} in Figure 15b that the contribution of M^f-to-N transitions in the photocycles of bR increases steadily for pH > 5.5. This supports our proposals for two different M^f-to-N transitions described by pK_a values of 5.6 (eq 10) and 7.5 (eq 19), respectively.

pH Dependence of M^f and M^s. As can be seen from the data in Figure 3, the decay of M can be fitted for each pH value by two different time constants and amplitudes. On this basis the two components M^f and M^s are defined. However, it turned out from the preceding analysis that each of these two M components involves pH-dependent subcomponents which stem from different cyclic reactions (Scheme I). The amplitudes of M^f and M^s therefore can be displayed

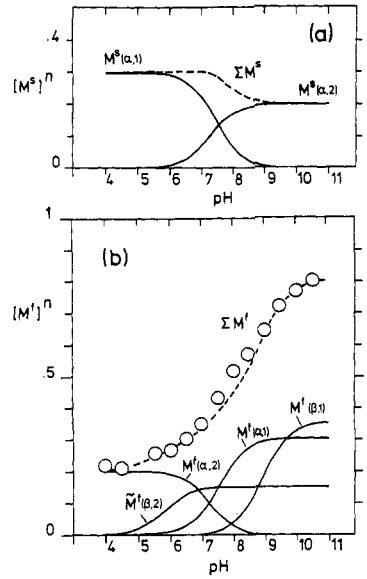

FIGURE 16: Normalized fractional concentrations of the various M components described in the text.

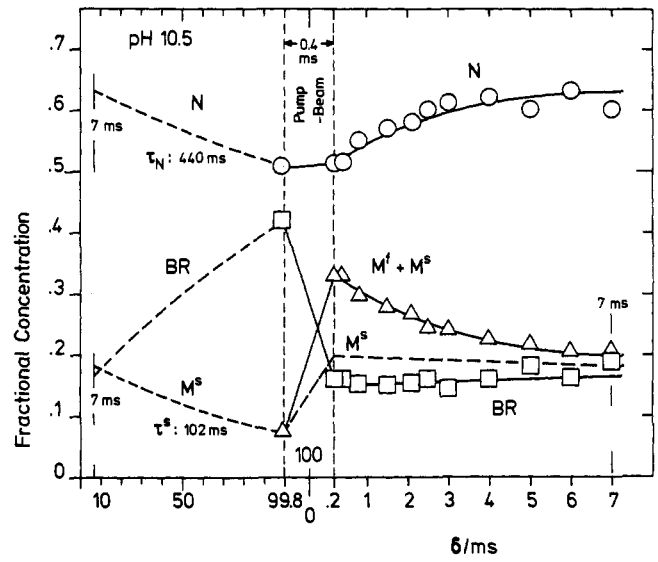

FIGURE 17: Data from a pump–probe RR experiment at pH 10.5 with a rotating cell. Other experimental conditions are as in Figures 2 and 9. Details are given in the text.

as

$$[M^f]_{pH} = \sum_i [M^f(i)]_{pH};\quad [M^s]_{pH} = \sum_i [M^s(i)]_{pH} \qquad (20)$$

where i denotes those species of bR which involve M^f or M^s intermediates in their cyclic reactions. The pH dependence of a single subcomponent is given by

$$[M^{f,s}(i)]_{pH} = [M^{f,s}(i)]_{max} f_i(pK_a(i)) \qquad (21)$$

where the first term gives the highest level which is reached at the low- or high-pH limit, and the f_i values are normalized titration-like functions determined by respective pK_a values. In analogy to eq 6 the first term is directly proportional to the fractional concentrations [bR(i)]. Since all $M^{s,f}$ subcomponents are rapidly formed ($\tau_2 \approx 80\ \mu s$) and decay slowly (several milliseconds), the proportionality factor in eq 6 is practically the same for all subcomponents and close to unity. With reference to ΔBR one obtains $[M^{f,s}(i)]^n_{max} = [bR(i)]$, where the index n indicates this normalization procedure. On this basis we calculated

$$[M^s]^n_{pH} = [bR(\alpha,1)][1 - f_0(pK_a\ 7.5)] + [bR(\alpha,2)]_{f_0}(pK_a\ 7.2) \qquad (22)$$

with $[bR(\alpha,1)] = 0.3$ and $[bR(\alpha,2)] = 0.2$ from eq 11 (cf. also Scheme I). In this relation f_0 is a titration-like function with a positive slope. The result is displayed in Figure 16a and shows that $[M^s]^n_{pH}$ is a rather smooth function of pH.

When $[M^s]^n_{pH}$ is combined with the experimental values for the relative amplitudes in Figure 3b, one obtains the data points for $[M^f]^n_{pH}$ which are inserted in Figure 16b as circles. The result demonstrates that $[M^f]^n_{pH}$ increases by a factor of 4 in the pH range 4–10.5. A good fit (dashed line in Figure 16b) to the data requires that besides the M^f components in bR(α,1), bR(α,2), and bR(β,2) (cf. Scheme I) an additional M^f component with a pK_a of 9.2 and a fractional concentration of 0.35 has to be introduced. This amplitude is equal to [bR-(β,1)], suggesting that, parallel to the titration of bR with pK_a = 9.2 (cf. first section in Results and Discussion), in the photocycle of bR(β,1) L is converted to M^f instead of to N_{fr} as at neutral pH (Scheme I). This is in line with observations in our RR experiments that at pH 10 L decays nearly completely to M on a time scale of 10 μs. At neutral pH the protein state P(N) which controls the formation of N is established in bR(β,1) within ~0.5 ms. This should also be the case at pH 10 and would imply that in the high-pH limit N is formed in bR(β,1) via M^f. This means that in this limit, according to Figure 16, ~80% of bR reacts through M^f and N and ~20% reacts through M^s.

It is the result of this section that the complex pH dependence of the decay of M as displayed in Figure 3 can be explained in a quantitative manner on the basis of Scheme I. This supports the validity of Scheme I.

Pump–Probe RR Experiment at pH 10.5: A Way To Check Scheme I. Fundamental conclusions on the reaction mechanism of bR can be obtained from the RR experiments we have carried out at pH 10.5 using a spinning cell (Figure 17). Under such conditions the lifetimes of N and M^s are 440 and 102 ms, respectively, so that the two intermediates are only partially reconverted to BR_{570} in a single rotational period (T_r = 100 ms).

Typical RR spectra recorded under such conditions are depicted in Figure 12 of Diller and Stockburger (1988). In the present work we recorded RR spectra in the C=C stretching region for delay times between 0.2 and 7 ms and for δ = 99.8 ms, i.e., just before a sample element reenters the pump beam. For excitation at 476 nm the spectra consist of contributions from BR_{570}, M, and N. The intermediate L is not accumulated since it decays rapidly to M (~7.5 μs). The fractional concentrations $[C(i)]$ were obtained from the relation

$$[C(i)] = f_i \bar{I}_{RR}(i) / \sum_i [f_i \bar{I}_{RR}(i)] \qquad (23)$$

where i refers to BR_{570}, M, and N and $\bar{I}_{RR}(i)$ refers to the relative RR intensities of these species. These quantities were inferred, as described earlier, from the RR bands in the C=C stretching region. For the factors f_i we used $f_M = 1$ and $f_N = 1.5$ as in Figure 9 ($f_{BR} = 1$ by definition). The results are summarized in Figure 17.

It can be seen that N fluctuates only slightly during a single period from an upper level $[\bar{N}] = 0.63$ to a lower level $[\underline{N}] = 0.51$. The two M components can be easily distinguished. Thus, the decay of M^f immediately sets in after the pump event with $\tau^f \approx 3$ ms and can be correlated with the synchronous increase of N. The residual fraction of M can

be attributed to M^s ($\tau^s \approx 102$ ms). In the pump beam the formation of M "immediately" follows the photolysis of BR_{570} which is due to the rapid formation of M ($\sim$7.5 μs) at pH 10.5. On the other hand, N does not change its concentration during the pump event, which means that secondary photoreactions of N are not efficient.

The observed phenomena can be described by two independent reaction sequences, which can formally be written as $BR \rightarrow M^f \rightarrow N \rightarrow BR$ and $BR \rightarrow M^s \rightarrow BR$ and are related to fractional concentrations [bR(N)] = [bR(α,1)] + [bR(β,1)] + [bR(β,2)] and [bR(M^s)] = [bR(α,2)] (cf. Scheme I). In order to deduce quantitative values, consideration of the experiment in Figure 17 is necessary.

It can be shown that in the sample element which has passed the pump beam n times the relative concentration of an intermediate i with respect to [bR(i)] is given by

$$[\bar{S}_n(i)] = \sum_{n=1}^{n} X[a(1-X)]^{n-1} \qquad (24)$$

where $X \equiv \Delta BR$, and $a = e^{-T_f/T_l}$ is an exponential factor which describes the decay of the intermediate i in the dark during the rotational period (T_r). In the limit $n \rightarrow \infty$ one obtains the equilibrium values

$$[\bar{S}(i)] = X/[1-a(1-X)], \quad [\underline{S}(i)] = a[\bar{S}(i)] \qquad (25)$$

From Figure 17 it can be concluded that $X \equiv \Delta BR \approx 0.6$, τ_N = 440 ms, and τ^s = 100 ms. Under such conditions it follows from eq 24 that the equilibrium in eq 25 is established within a few rotational periods (T_r = 100 ms) of the cell, i.e., in less than 1 s. On the other hand, the diffusion time of membrane patches out of the illuminated cylindrical ring is >10 s (Diller & Stockburger, 1988). This implies that bR is probed in the equilibrium state of eq 25. One thus obtains

$$[\bar{S}(N)] = 0.881; \quad [\underline{S}(N)] = 0.701$$

$$[\bar{S}(M^s)] = 0.706; \quad [\underline{S}(M^s)] = 0.265 \qquad (26)$$

The fractional concentration of bR(N) is given by [bR(N)] = $[\bar{N}][\bar{S}(N)]^{-1}$; the fractional concentrational of bR(M^s) is obtained similarly. With $[\bar{N}]$ = 0.63 and $[\bar{M}^s]$ = 0.2 from Figure 17 and eq 26 one obtains

$$[bR(N)] = 0.72, \quad [bR(M^s)] = 0.28 \qquad (27)$$

These results have to be compared with the respective values of 0.8 and 0.2 obtained in the previous section from the amplitudes of M^f and M^s in the high-pH limit. In view of the entirely different methods by which the data were obtained, the agreement is fairly good. The RR experiments in Figure 17 strongly favor our model in which M^f and N on the one side and M^s on the other side occur in independent photocycles. In the following this view will be further supported by the exclusion of other models.

Conformational Changes of the Protein Backbone in M^f and M^s. We have argued above that a conformational transition of the protein backbone from state P(L) to state P(N) is a necessary condition for the appearance of the N chromophore in the photocycle. Consequently, in all reaction sequences $L \rightarrow M^f \rightarrow N$ the transition between the two protein states has to take place during the lifetime of M^f. This would define two different M states, M^f[P(L)] and M^f[P(N)]. Remember that the time constant for the conversion of P(L) to P(N) was found to be $\sim$0.5 ms in bR(β,1) where it is directly reflected by the L $\rightarrow$ N transition (Scheme I). A similar value should be expected for the P(L) $\rightarrow$ P(N) conversion in the M^f state. It can further be concluded that the P(N) state favors the reprotonation of the Schiff base in the $L \rightarrow M^f \rightarrow N$ sequences. On the other hand, it is suggested that in those subspecies of bR which have M^s states but no N in their cyclic reactions (Scheme I) the protein state P(N) is not established and the reprotonation of the Schiff base cannot occur in the M^s state.

Other Models to Explain M^f and M^s. In order to explain the biphasic decay of M, a branching reaction in the photocycle has been proposed (Li et al., 1984; Maurer et al., 1987b). The question is whether our results at pH 10.5 (Figure 17), where the two M states can be easily distinguished, might be explained by such a model. This would mean that the two independent sequences $BR \rightarrow M^f \rightarrow N \rightarrow BR$ and $BR \rightarrow M^s \rightarrow BR$ we had invoked to explain the results of the experiment in Figure 17 would be the two branches of a single photocycle according to

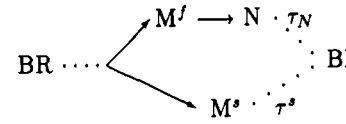

(28)

This scheme can be modeled by dividing ΔBR into two fractions whose relative magnitudes are given by the amplitudes of M^f and M^s ([M^f]:[M^s] = 4:1 at high pH; cf. Figures 3b and 16). On this basis we calculated with the experimental data in Figure 17 (ΔBR = 0.6; τ_N = 440 ms, τ^s = 102 ms) the mean value (averaged over a single rotational period) for [N]/[M^s] in eq 28 in the stationary state. A value of 16.5 was obtained, compared to 4.2 deduced from the experimental data in Figure 17. This discrepancy indicates that the branching model cannot explain the experimental results and therefore can be definitively excluded.

Another interesting model to explain the biphasic decay of M was proposed by Otto et al. (1989) and Ames and Mathies (1990). It is based on the observation that for pH > 8 the lifetimes of both N and M^s increase with increasing pH. It was proposed that in a linear photocycle an M $\leftarrow$ N back reaction takes place so that an intermediate quasistationary equilibrium, M $\rightleftharpoons$ N, is established during the long lifetime of N. In this model the fast decay of M is associated with the establishment of the intermediate M $\rightleftharpoons$ N equilibrium so that $\tau^f = (k_{MN} + k_{NM})^{-1}$, whereas the slow decay of M would be determined by the slow decay of N. In other words, τ^s should be equal to τ_N. This, however, is not found. For instance, in the experiment of Figure 17 (pH 10.5) τ_N is 4.4 times longer than τ^s.

Additional evidence for the inequality of τ_N and τ^s in the range pH 8–10 is provided by Figure 18. There, the data for τ_N (pH $\geq$ 8) were obtained from optical transient experiments at 640 nm. It can be estimated from the absorption spectra of N and BR_{570} (Drachev et al., 1987) that at 640 nm $\epsilon_{BR} \approx 2\epsilon_N$. The long-lived transient observed at this wavelength therefore can be attributed to the decay of N. For comparison, the pH dependence of τ^s is indicated in Figure 18 by the dashed line. It can be seen that for pH $\geq$ 8 τ_N is larger than τ^s by factors of 2–5. This behavior can be also inferred from the work by Kouyama et al. (1988; cf. Figures 4 and 7). We therefore conclude on the basis of the various experimental evidences that the biphasic decay of M cannot be explained by an intermediate M $\rightleftharpoons$ N equilibrium.

Back Reactions in a Homogeneous Cycle. Until now it has been widely accepted that bR is a homogeneous species. This would imply that each bR molecule undergoes the same reaction pathway (homogeneous cycle). In order to account

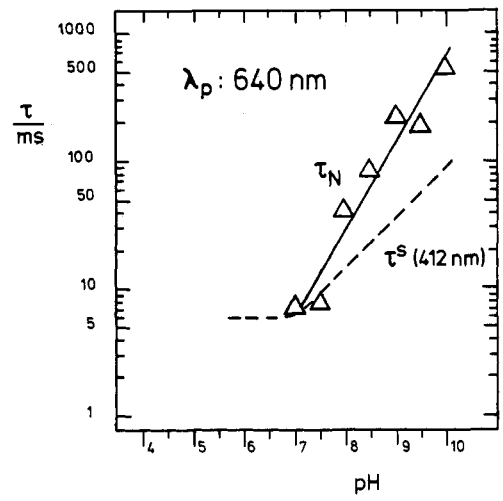

FIGURE 18: Decay time, τ_N, obtained from optical transients at 640 nm for pH ≥ 8 at 20 °C. The two values at neutral pH were deduced from RR experiments. For comparison, the pH dependence of τ^s (Figure 3) is inserted as a dotted line. At alkaline pH τ^s is significantly lower than τ_N. At neutral pH τ^s approaches τ_N.

for the observed kinetic phenomena, which do not fit into a homogeneous sequential cycle, reversible reaction steps were proposed by various authors (Ames & Mathies, 1990; Váró & Lanyi, 1991a–c; Chernavskii et al., 1989).

For principal reasons back reactions cannot be excluded a priori. The question, however, is whether they are efficient enough to account for the observed phenomena. Thus, in the previous section it was shown that a potential back reaction, M ← N, cannot be responsible for the observed biphasic decay of M.

It was proposed by Ames and Mathies (1990) that the biphasic decay of L is reproduced in a homogeneous scheme by introducing an L ← M back reaction. However, it can be seen from the data in Figure 9 that for pH 7.6 such a step cannot be very efficient, since for $\delta > 1$ ms L has completely disappeared, whereas M still has a significant amplitude. This phenomenon has been invoked by Váró and Lanyi (1991b) to postulate a single irreversible step in their homogeneous scheme.

On the other hand, it is tempting to attribute the kinetic behavior of L and M we found for pH 5 (Figure 10) to the establishment of an intermediate L ⇌ M equilibrium. Thus, the slow parallel decay of L and M might suggest that L is strongly coupled to M. This explanation was indeed favored in our earlier work (Alshuth & Stockburger, 1986). However, in the light of our new kinetic and structural information from pH-dependent experiments, we came to a completely different conclusion in the present study, namely, that at pH 5 in a fraction of bR (bR(β)) the decay of L is significantly delayed.

In this context we wish to mention a relaxation experiment we carried out in our laboratory (Diller, 1988). In this experiment a fraction of M (~50%) was reconverted to BR_{570} by blue light at a delay time of 400 μs after photolysis; 200 μs after blue light excitation, no equilibration of N and M could be identified. This shows that under such conditions N and M are not coupled to each other.

The finding that back reactions in the photocycle of bR are not very efficient is understandable from a more general point of view. Thus, one has to consider that the intermediate states which can be identified via the chromophore are "selected metastable states" of the entire system: chromophore plus protein matrix. A transition from a certain metastable state to the following one in the reaction sequence then must go through a variety of short-lived substates of the entire system. Whereas back reactions between such substates may have a significant probability, one would expect that each of the selected metastable states has a somewhat lower free energy than its metastable precursor so that back reactions between such metastable states have a low probability.

CONCLUSIONS

So far we have been concerned with establishing a reaction scheme which accounts for the complex kinetic behavior of bR. In this section the various reaction steps which are involved in this scheme and which are important for the biological function will be analyzed. It will be seen that the basic reaction steps (e.g., isomerization and proton translocation) in the various photocycles underlie the same mechanisms.

Reconstitution of BR_{570}. We first consider the "reconstitution phase" in sequences with M intermediates. This starts with the decay of M and ends with the recovery of BR_{570} and involves the reprotonation of the Schiff base and the reisomerization of the retinal chain as the essential steps. At pH 7 the three reconstitution pathways $M^f \rightarrow N \rightarrow BR$, $M^f \rightarrow O \rightarrow BR$, and $M^s \rightarrow BR$ can be distinguished (cf. Scheme I). For pH > 7.5 the recovery of BR_{570} is significantly slowed down with increasing pH (Figures 15 and 18). Let us first consider the reconstitution via N, which can be displayed in the form

$$\text{pH} > 7.5: \quad M^f \xrightarrow[\tau_N]{\tau^f} N \xrightarrow{[H^+]} BR \qquad (29)$$

where $[H^+]$ stands for the proton concentration in the aqueous phase. In this case the reprotonation of the Schiff base precedes the reisomerization of retinal. Since τ^f is practically independent of pH (cf. Figure 3), the Schiff base must be reprotonated from an internal donor. On the other hand, the drastic decrease of τ_N for pH > 7.5 (Figure 18) suggests that the reisomerization step is controlled by the uptake of a proton from the aqueous phase. In the "diffusion-controlled limit" the rate for the reaction of a proton in the aqueous phase with a molecular species (e.g., a conjugated base) is given by $k_d = k_r[H^+]$, with a typical value of $k_r \approx 4 \times 10^{10}\ M^{-1}\ s^{-1}$ (Eigen et al., 1961). It can be concluded from the data in Figure 18 that, for pH → 10, $k_N(\equiv 1/\tau_N)$ approaches the diffusion-controlled rate, k_d. This means that in the high-pH limit the rate-limiting step for the reisomerization process is the diffusion of a proton to the membrane surface, and that each proton which is trapped there initiates the process. On the other hand, in the low-pH limit (pH < 7.5) τ_N approaches a lower level of a few milliseconds which is independent of pH.

Following the generally accepted idea that in the first phase of the photocycle a proton is ejected to the extracellular side and in the reconstitution phase a proton is taken up from the cytoplasmic side, the observed behavior can be modeled in the following way. At the cytoplasmic surface of the protein molecule there exists at least one specific binding site for a proton (trap). In the interior of the protein, maybe close to the chromophore, there exists another specific binding site for protons which we call the "internal reactive site" (irs). Before N is formed the irs is empty. During the lifetime of N a proton migrates from the cytoplasmic surface trap to the irs. Once this is occupied by a proton, the isomerization sets in. It is conceivable that the proton uptake primarily induces a conformational change of the protein backbone, which is followed by the reisomerization. At low pH (<7.5) the surface trap is always populated. In this limit τ_N is determined by

the time of proton needs to migrate from the surface (probably through a proton conduction channel) to the irs plus the time for the isomerization itself. In the high-pH limit the surface trap is empty so that the process becomes diffusion-controlled.

It thus turns out that in the reconstitution process via $M^f \rightarrow N$ (eq 29) two distinct proton translocation processes are involved, namely, the reprotonation of the Schiff base from an internal donor group and the uptake of a proton from the cytoplasmic surface, which catalyzes the reisomerization process.

Now we consider those recovery processes in which N is not formed. In Scheme I two cases occur in which the reconstitution starts from M^s. These processes can be formally written as

$$\text{pH} < 7.5: \quad M^s \xrightarrow[\tau^S]{} BR; \qquad \text{pH} \gg 7.5: \quad M^s \xrightarrow[\tau^S]{[H^+]} BR \tag{30}$$

It is suggested that in both cases the same reconstitution mechanism takes place. In the high-pH limit the decay of M^s strongly decreases with increasing pH (cf. Figure 3), and it could be shown that this process is catalyzed by the diffusion-controlled uptake of a proton from the aqueous phase (Otto et al., 1989). This demonstrates that a proton migrates from the cytoplasmic surface to the active site to induce the recovery of BR_{570} from M^s. The problem is now to resolve the sequential order of reprotonation and reisomerization during the M^s-to-BR recovery and to ask which of the two processes is catalyzed by the uptake of an external proton. Since N is not involved in this process, it can be excluded that reprotonation of the Schiff base precedes the reisomerization as in eq 29. The recovery therefore can be described in the form

$$M^s_{13\text{-}cis} \xrightarrow{\text{reisomerization}} M^*_{trans} \xrightarrow{\text{reprotonation}} BR_{570} \tag{31}$$

where M^*_{trans} is an intermediate of the chromophore in all-*trans* configuration with a deprotonated Schiff base. The alternative is now whether the proton which is taken up from the cytoplasmic side catalyzes reisomerization or simply serves for reprotonation of the Schiff base. Let us assume that the latter would be the case. This would imply that in the high-pH limit the reprotonation would be the rate-limiting step and M^*_{trans} would be accumulated during the cycle. Since distinct differences in the RR spectra of M^*_{trans} and $M_{13\text{-}cis}$ can be expected, M^*_{trans} should be found in RR experiments at high pH. This, however, is not the case: We therefore conclude that it is the reisomerization which is catalyzed by the uptake of a proton and at high pH is the rate-limiting step.

This conclusion is supported by a comparison of the "thermal" with the "blue-light-induced" recovery of BR_{570} from M. This latter phenomenon has been frequently described in the literature [see, for instance, Oesterhelt and Hess (1973), Ormos et al. (1980), and Butt (1990)]. In the course of the light-induced back reaction from M to BR_{570} an intermediate state, M*, is formed which decays thermally to BR_{570} with a time constant of $\approx$150 ns at room temperature and pH 7 (Kalisky et al., 1978, 1981). It was inferred from time-resolved RR studies that M* is isomerized to the all-*trans* configuration of retinal (Stockburger et al., 1979). This means that once the light-induced isomerization of the retinal chain is accomplished (within a few picoseconds), the reprotonation of the Schiff base follows "instantaneously" (150 ns), i.e., from an internal proton donor group. The recovery of BR_{570} from M^s thus can be displayed in the general form

$$M^s_{13\text{-}cis} \xrightarrow[(h\nu)]{(H^+),\tau^S} M^*_{trans} \xrightarrow{\ll\tau^S} BR_{570} \tag{32}$$

where (H^+) means that *cis–trans* isomerization is catalyzed by the occupation of an internal reactive site (irs). Hence, in the dark the rate-limiting step in eq 32 is the proton-induced reisomerization. In the case of light-induced *cis–trans* isomerization the rate is limited by the speed of the reprotonation of the Schiff base.

The recovery of BR_{570} in the sequence $M^f \rightarrow O \rightarrow BR$ in our interpretation would be a special case of eq 32 in which O is placed between M^*_{trans} and BR_{570} and the irs is populated from an internal group A_uH.

In summary we conclude that in all recovery processes the reisomerization step is catalyzed by the protonation of an internal reactive site, whereas the reprotonation of the Schiff base occurs from an internal donor. It is only the sequence of the two processes which is different. This behavior may be explained by the different stability of the M state in the various subspecies of bR. Thus, we have argued above that the reprotonation of the Schiff base ($M^f \rightarrow N$) requires that the protein state P(N) is established. Our analysis further suggests that the reprotonation of the Schiff base, i.e., the formation of N, is not a prerequisite for the spontaneous reisomerization of retinal on a millisecond time scale as had been proposed (Tavan et al., 1985). This is corroborated by the observation that at high pH, where a proton for the occupation of the irs is not available, the N state has a lifetime of severals seconds (Kouyama et al., 1988).

In the photocycle of the subspecies $bR(\beta,1)$ the intermediate M is not formed, and the reconstitution of BR_{570} can be described by the sequence $L \rightarrow N \rightarrow BR$. From the discussion above it can be concluded in this case also that the reisomerization is catalyzed by the uptake of an external proton.

Functionally Important Residues. Before we discuss our own conclusions further, a brief review of the current ideas on the role of functionally important residues is appropriate. In the structural model of Henderson et al. (1990) the Schiff base is connected to the extracellular surface by a fairly open hydrophilic channel and to the cytoplasmic side by a narrow, more hydrophobic pore. Three functionally important residues (Asp-85, Asp-212, and Arg-82) are located in the extracellular channel a few angstroms "below" the Schiff base, whereas another key residue, Asp-96, is found in the cytoplasmic pore about 10 Å "above" the Schiff base.

The first evidence for a negative counterion to the positively charged Schiff base in BR_{570} was inferred from the acid-induced transition of the purple chromophore (BR_{570}) to a blue form (BR_{605}) [$pK_a \approx 3$; cf. Mowery et al. (1979)]. It was proposed by Fischer and Oesterhelt (1979) that the formation of the blue form is due to the neutralization of a carboxylate group which is located in the vicinity of the Schiff base.

The identity of the counterion could be determined in experiments with site-specific mutants of bR. It was found that the formation of a purple chromophore which is active in proton pumping requires a negatively charged carboxylic side chain at residue 85, whereas a neutral side chain at this position leads to the functionally inactive blue chromophore (Butt et al., 1989; Otto et al., 1990; Subramaniam et al., 1990). Further support for the role of Asp-85 as the proximal counterion can be inferred from the observation that the protonated Schiff base is significantly destabilized when Asp-85 is replaced by the neutral residue Asn (Otto et al., 1990). On the other hand, it was found that the purple chromophore is also formed when the neighboring charged residues Asp-

212 and Arg-82 are substituted by neutral residues (Otto et al., 1990; Rothschild et al., 1990). These observations imply that of all the charged residues in the vicinity of the Schiff base it is the carboxylate side chain of Asp-85 which comes closest to the Schiff base and therefore has a direct influence on the color and the function of the chromophore.

Nevertheless, the side chain of Asp-85 cannot be in direct contact (hydrogen bonding) with the Schiff base. Thus it was found that a few tightly bound water molecules are located in the immediate environment of this group (Hildebrandt et al., 1984; Papadopoulos et al., 1990). This view is corroborated by NMR studies (de Groot et al., 1989, 1990).

The prominent role of Asp-85 as a counterion also becomes evident from a comparison of the RR spectra of the active purple (BR_{570}) and the inactive blue (BR_{605}) chromophore. This reveals that in BR_{570} the structure is well defined (all-*trans*) and homogeneous, whereas in BR_{605} the chromophore adopts different configurational (all-*trans*, 13-*cis*) and conformational states (Massig et al., 1985).

Microscopic evidence for the function of Asp-85 as the primary acceptor of the Schiff base proton in the L-to-M transition was provided by a series of infrared experiments. Thus a positive peak at $\sim$1762 cm^{-1} in the M–BR difference spectra which appears synchronously with M could be correlated with the carbonyl stretching vibration of an aspartic acid residue which becomes protonated in the L-to-M transition (Siebert et al., 1982; Engelhard et al., 1985). In static FTIR experiments in conjunction with site-directed mutagenesis the 1762-cm^{-1} band could be assigned to the carbonyl band of the protonated carboxylic side chain of Asp-85 (Braiman et al., 1988). The acceptor function of Asp-85 is further supported by the observation that the M state is only formed when a deprotonated carboxylic group exists at residue 85 (Otto et al., 1990).

It was found that the residue Asp-96 plays an important role in the reconstitution mechanism of bR. Thus, in mutants of bR where Asp-96 is substituted with Asn, Ala, or Gly, the rates of the photocycle and of the proton pump are dramatically reduced (Butt et al., 1989; Holz et al., 1989; Tittor et al., 1989). This has stimulated the idea that the carboxylic side chain of Asp-96 might act as an internal proton donor for the reprotonation of the Schiff base (Otto et al., 1989; Miller & Oesterhelt, 1990). In the following a different mechanism will be proposed.

Asp-85 Is the Internal Donor for the Reprotonation of the Schiff Base. Here we propose that the donor for the reprotonation of the Schiff base is the Asp-85 residue which had been protonated in the preceding L-to-M transition. In the case where reprotonation leads to the formation of N, this proposal is based on the following arguments.

It was outlined earlier in this paper that the direct L $\rightarrow$ N transition in the photocycle of bR(β,1) (Scheme I) is a consequence of the conformational transition in the protein backbone described by Ormos (1991) [see also Ormos et al. (1992) and Cao et al. (1993)]. From a comparative analysis of the RR spectra in the present paper we have concluded that in N, like in L, Asp-85 is the negative counterion and thus is deprotonated. In the reaction sequence L $\rightarrow$ M^f $\rightarrow$ N the N state appears after de- and reprotonation of the Schiff base. In this case the protein transition apparently takes place in the M^f state. Since, as is well established, the L $\rightarrow$ M^f reaction step is accompanied by the protonation of Asp-85 and, according to our own conclusions, Asp-85 is deprotonated in N, it is suggested that in the M^f $\rightarrow$ N reaction step the Schiff base is directly reprotonated from Asp-85.

When samples under identical conditions were studied in optical and infrared transient experiments, it was found that the decay of the 1762-cm^{-1} carbonyl band matches the decay of the absorbance of M at 412 nm (Siebert et al., 1982; Gerwert et al., 1990). Since the decay of M indicates the synchronous protonation of the Schiff base, this finding is in line with a direct reprotonation of the Schiff base from Asp-85.

In summary, we have presented different arguments which support the idea that in all reaction pathways which involve the M intermediate the Schiff base is reprotonated directly from Asp-85. In this model Asp-85 acts both as acceptor and donor for the Schiff base proton.

Excursion into Infrared Spectroscopy. Here we briefly discuss recent FTIR studies on bR concerning the role of the key residues Asp-85 and Asp-96. In the L–BR difference spectrum at low temperature (170 K) a negative peak at 1742 cm^{-1} and a positive one at 1748 cm^{-1} were assigned to carbonyl vibrations of Asp-96 (Braiman et al., 1988). It was proposed by Gerwert et al. (1989) that in L, like in BR_{570}, Asp-96 is protonated but undergoes an environmental change, giving rise to a frequency shift of the carbonyl stretch from 1742 to 1748 cm^{-1}. This interpretation seems to be in contradiction with the observation that at higher temperatures the positive peak at 1748 cm^{-1} is missing, which leads to the conclusion that Asp-96 is deprotonated in L (Chen & Braiman, 1991; Ormos et al., 1992). In the light of the present paper, a resolution of this problem could be that the two L chromophores (L_{fd} and L_{sd} in eqs 3 and 5) which we had attributed to different species of bR behave in a way that Asp-96 is protonated in L_{fd} but deprotonated in L_{sd}. This could explain the result of Ormos et al. (1992) that under conditions where the transition L_{fd} $\rightarrow$ M is already accomplished but L_{sd} is not yet converted to N (240 K) only the negative peak at 1742 cm^{-1} appears in the L–BR difference spectrum. The appearance of the positive peak at 1748 cm^{-1} at 170 K could be explained by the fact that at this temperature M is not yet formed, so that L_{fd} is the dominating L chromophore (L_{fd}:L_{sd} $\sim$ 65:35 at neutral pH; cf. Scheme I).

It could be shown that the N–BR difference spectra contain as a chracteristic feature a positive/negative band pair of nearly equal intensity at 1755/1742 cm^{-1}, respectively (Pfefferlé et al., 1991; Ormos et al., 1992). Whereas the negative peak at 1742 cm^{-1} can be correlated with Asp-96, the assignment of the positive peak at 1755 cm^{-1} is more complicated. It was proposed by Braiman et al. (1991) that the band at 1755 cm^{-1} is due to the protonated state of Asp-85, which undergoes an environmental change during the M–N transition, shifting the carbonyl band from 1762 cm^{-1} in M to 1755 cm^{-1} in N. On the basis of this interpretation, the negative peak at 1742 cm^{-1} was taken as evidence that Asp-96 is deprotonated in N, whereas Asp-85 remains in the protonated state. It was further concluded that Asp-96 acts as the proton donor in the reprotonation pathway of the Schiff base (Braiman et al., 1991; Bousché et al., 1991).

This model is in contradiction to our proposal for a direct reprotonation of the Schiff base from Asp-85. Thus, an alternative interpretation of the band pair 1755/1742 cm^{-1} in N is required. Here we propose that Asp-96 is protonated in N but undergoes a shift of its carbonyl stretch from 1742 cm^{-1} in BR_{570} to 1755 cm^{-1} in N. This interpretation is in close analogy to the one proposed for the intermediate L (L_{fd}) (Gerwert et al., 1989). The bigger shift may be due to the protein transition P(L) $\rightarrow$ P(N) which precedes the formation of N. Interesting phenomena in the C=O streching region of Asp-96 and Asp-85 were reported by Braiman et al. (1991).

They found that on a time scale of ≈1 ms (20 °C, neutral pH) a distinct positive peak arises at 1755 cm^{-1} [this effect had been reported earlier by Siebert et al. (1982)]. It was noted that this peak appears to evolve from the positive carbonyl band of protonated Asp-85 at 1762 cm^{-1} which refers to the M state, and that both peaks subsequently decay in parallel on a time scale of several milliseconds. From this behavior it was concluded that Asp-85 remains protonated but undergoes a frequency shift from 1762 to 1755 cm^{-1}.

In the light of the present study we propose a somewhat different interpretation. Above we had attributed the band pair 1755/1742 cm^{-1} in the N–BR difference spectra to a frequency shift of the carbonyl band in protonated Asp-96. On a time scale of ~1 ms one would expect that, due to the transition $L_{sd} \rightarrow N_{fr}$ (eq 3), the intensity at 1755 cm^{-1} increases, whereas the negative peak at 1742 cm^{-1} remains unchanged (we have argued above that L_{sd} is characterized by a single negative peak at 1742 cm^{-1} in the difference spectrum). On the other hand, one might also expect on a 1-ms time scale intensity shifts of the carbonyl band of Asp-85 which are caused by the protein transition P(L) → P(N) in the M^f state of a reaction sequence L → M^f → N. This could explain the observed intensity shift from 1762 to 1755 cm^{-1}. This explanation would imply that in the P(N) protein state the carbonyl bands of Asp-96 and Asp-85 both lie at nearly the same position (~1755 cm^{-1}).

The parallel decay of the two peaks at 1762 and 1755 cm^{-1} in terms of our model would reflect the decay of M^s to BR_{570} and of N to BR_{570} in parallel cycles with time constants of τ^s and τ_N, respectively (Scheme I).

The Role of Asp-96. There is convincing evidence that Asp-96 plays a key role in the reconstitution of BR. This has raised the idea that its function is that of a proton donor in the reprotonation pathway of the Schiff base. However, in this paper we have argued that the Schiff base is directly reprotonated from Asp-85. This suggests that Asp-96 might be involved in the reisomerization process which, as we have proposed above, is triggered by the uptake of a proton from the cytoplasmic side. In this model Asp-96 would be integrated in a hydrogen-bonding chain and would control the conduction of protons from the cytoplasmic surface to an internal reactive site (see Scheme II: there Asp-96 is attributed to the group A_zH). In the reconstitution pathway $M^f \rightarrow O \rightarrow BR$ (eqs 15 and 16) we had proposed that this site is protonated from an internal donor. It might be that in this special case (~20% of bR; cf. Scheme I) Asp-96 takes in this donor function.

A Model for Proton Pumping. Molecular models for proton pumping which are presently discussed in the literature are all based on the idea that the Schiff base acts as an "active proton transfer switch" (Schulten & Tavan, 1978). So it was proposed that in the L → M transition the Schiff base donates a proton to Asp-85 as the primary acceptor on the extracellular side and in the subsequent M → N transition takes up a proton from Asp-96 on the cytoplasmic side. Molecular details which account for the energetics and vectoriality of the pump were described in the various reports (Braiman et al., 1988; Henderson et al., 1990; Mathies et al., 1991; Rothschild et al., 1992; Oesterhelt et al., 1992; Lanyi, 1992).

In Scheme II the de- and reprotonation of the Schiff base and of the hypothetically introduced internal reactive site (irs) are combined with the temporal evolution of the chromophore in two different types of reaction pathways (cf. eqs 29 and 32). Note that the irs was introduced to account for the proton-induced reisomerization of retinal. Scheme II can be considered as a basic model for the proton pump: on the time scale of the L-to-M transition a proton is released from the irs to the extracellular side, and the decay of N (Scheme IIa) or M^s (Scheme IIb) is coupled to the uptake of a proton by the irs from the cytoplasmic side. In this model the proton which is pumped passes through the irs and not through the Schiff base as in the switch models.

Scheme II: Two Different Reaction Pathways of the Photocycle[a]

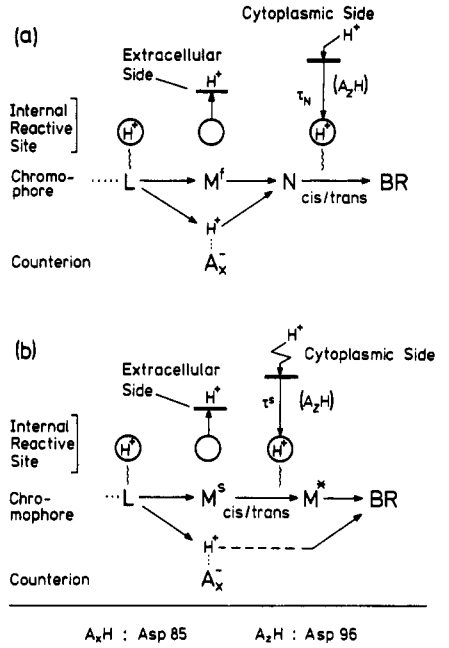

[a] (a) Reprotonation of the Schiff base precedes reisomerization. (b) Reisomerization precedes reprotonation. These pathways are combined with proton-transfer reactions as described in the text.

In spite of the principal difference between our model and the switch models, the proton release during the L → M transition is described in both cases in a similar way. This is not surprising since every model has to account for the observation that, synchronously with the L → M transition, a proton appears at the extracellular surface (Heberle & Dencher, 1990, 1992). This suggests a strong coupling between the deprotonation of the Schiff base and the ejection of a proton which might be mediated by a secondary proton donor. In the models of Mathies et al. (1991) and Braiman et al. (1988) the secondary donor was attributed to the guanidinium side chain of Arg-82. In our model this role might be played by the irs. However, the question arises whether the proton ejection is coupled at all to the deprotonation of the Schiff base or whether there is only an "accidental coincidence" between these two events. This latter point of view is corroborated by the following arguments. We found that under normal conditions (pH 6–8) 35% of the bR molecules go through a cyclic reaction in which M is not formed [bR-(β,1) in Scheme I]. Since on the average in each cycle a proton is pumped [for a discussion, see Schneider et al. (1989)], it is suggested that this is also the case in the cycle of bR(β,1) in which M is not formed. This would mean that the vectoriality of the proton pump cannot be correlated with the de- and reprotonation of the Schiff base as proposed in the switch models.

Here we propose that the vectorial behavior is largely controlled by conformational changes of the protein backbone during the cyclic reaction. This view is corroborated by the observation of such changes by FTIR (Rothschild, 1992) and other techniques (Ort & Parson, 1979; Koch et al., 1991).

After the primary photochemical event, excess energy is stored in the intermediate K (Birge et al., 1991; Rohr et al., 1992) which is used for functionally important rearrangements of the chromophore and its environment during the transition from K to L. This can be concluded from RR spectroscopic evidence (Lohrmann et al., 1991; Lohrmann & Stockburger, 1992) and time-resolved dichroism measurements (Wan et al., 1991). Then at the stage of L the system as a whole is prepared for the decisive subsequent reaction steps. We propose that in L a unidirectional proton conduction channel from the irs to the extracellular side is prepared which guarantees the vectorial release of a proton to this side of the membrane. A model for the molecular structure and function of such a channel has been recently proposed by Olejnik et al. (1992).

At the stage of M (or during M → N) a second unidirectional conduction channel from the cytoplasmic surface to the irs would be opened so that a proton could diffuse in a few milliseconds from the cytoplasmic surface to the irs. The formation of this channel might be correlated with the P(L) → P(N) protein transition first described by Ormos (1991). Once the irs is occupied, reisomerization sets in. Then the cytoplasmic channel would be closed, and the original BR_{570} state would be reconstituted.

ACKNOWLEDGMENT

Purple membranes were a gift from the laboratory of D. Oesterhelt, which is greatly acknowledged. In particular we thank J. Tittor for providing us with the sample.

REFERENCES

Alshuth, T., & Stockburger, M. (1986) *Photochem. Photobiol. 43* (1), 55–66.

Ames, J. B., & Mathies, R. A. (1990) *Biochemistry 29*, 7181–7190.

Balashov, S. P., Govindjee, R., & Ebrey, T. G. (1991) *Biophys. J. 60*, 475–490.

Birge, R. R., Copper, T. M., Lawrence, A. F., Masthay, M. B., Zhang, Ch.-F., & Zidovetzki, R. (1991) *J. Am. Chem. Soc. 113*, 4327–4328.

Braiman, M. S., Mogi, T., Marti, T., Stern, L. J., Khorana, H. G., & Rothschild, K. J. (1988) *Biochemistry 27*, 8516–8520.

Braiman, M. S., Bousché, O., & Rothschild, K. J. (1991) *Proc. Natl. Acad. Sci. U.S.A. 88*, 2388–2392.

Bousché, O., Braiman, M., He, Y.-W., Marti, T., Khorana, H. G., & Rothschild, K. J. (1991) *J. Biol. Chem. 266* (17), 11063–11067.

Butt, H. J. (1990) *Eur. Biophys. J. 19*, 31–39.

Butt, H. J., Fendler, K., Bamberg, E., Tittor, J., & Oesterhelt, D. (1989) *EMBO J. 8* (6), 1657–1663.

Cao, Y., Váró, G., Klinger, A. L., Czajkowsky, D. M., Braiman, M. S., Needleman, R., & Lanyi, J. K. (1993) *Biochemistry 32*, 1981–1990.

Chen, W.-G., & Braiman, M. S. (1991) *Photochem. Photobiol. 54* (6), 905–910.

Chernavskii, D. S., Chizhov, I. V., Lozier, R. H., Murina, T. M., Prokhorov, A. M., & Zubov, B. V. (1989) *Photochem. Photobiol. 49* (5), 649–653.

Chizhov, I., Engelhard, M., Chernavskii, D. S., Zubov, B., & Hess, B. (1991) *J. Photochem. Photobiol. 61*, 1101–1106.

Dancsházy, Zs., Govindjee, R., Nelson, B., & Ebrey, T. G. (1986) *FEBS Lett. 209*, 44–48.

Dancsházy, Zs., Govindjee, R., & Ebrey, T. G. (1988) *Proc. Natl. Acad. Sci. U.S.A. 85*, 6358–6361.

de Groot, H. J. M., Harbison, G. S., Herzfeld, J., & Griffin, R. G. (1989) *Biochemistry 28*, 3346–3353.

de Groot, H. J. M., Smith, S. O., Courtin, J., van den Berg, E., Winkel, C., Lugtenburg, J., Griffin, R. G., & Herzfeld, J. (1990) *Biochemistry 29*, 6873–6883.

Diller, R. (1988) Ph.D. Thesis, University of Göttingen, Göttingen, Germany.

Diller, R., & Stockburger, M. (1988) *Biochemistry 27*, 7641–7651.

Dobler, J., Zinth, W., Kaiser, W., & Oesterhelt, D. (1988) *Chem. Phys. Lett. 144*, 215.

Doig, S. J., Reid, P. J., & Mathies, R. A. (1991) *J. Phys. Chem. 95*, 6372–6379.

Drachev, L. A., Kaulen, A. D., Skulachev, V. P., & Zorina, V. V. (1987) *FEBS Lett. 226* (1), 139–144.

Ehrenberg, B., Ebrey, T. G., Friedman, N., & Sheves, M. (1989) *FEBS Lett. 250* (2), 179–182.

Eigen, M., Kruse, W., Maass, G., & de Maeyer, L. (1961) in *Progress in Reaction Kinetics (II)* (Porter, G., Ed.) pp 286–318, Pergamon Press, London.

Engelhard, M., Gerwert, K., Hess, B., Kreutz, W., & Siebert, F. (1985) *Biochemistry 24*, 400–407.

Fischer, U., & Oesterhelt, D. (1979) *Biophys. J. 28*, 211–230.

Fodor, S. P. A., Ames, J. B., Gebhard, R., van den Berg, E. M. M., Stoeckenius, W., Lugtenburg, J., & Mathies, R. (1988) *Biochemistry 27*, 7097–7101.

Frauenfelder, H., Parak, F., & Young, R. D. (1988) *Annu. Rev. Biophys. Biophys. Chem. 17*, 451–479.

Gerwert, K., Hess, B., Soppa, J., & Oesterhelt, D. (1989) *Proc. Natl. Acad. Sci. U.S.A. 86*, 4943–4947.

Gerwert, K., Souvignier, G., & Hess, B. (1990) *Proc. Natl. Acad. Sci. U.S.A. 87*, 9774–9778.

Groma, G. I., & Dancsházy, Zs. (1986) *Biophys. J. 50*, 357–366.

Grossjean, M. F., Tavan, P., & Schulten, K. (1990) *J. Phys. Chem. 94*, 8059–8069.

Hanamoto, J. H., Dupuis, P., & El-Sayed, M. A. (1984) *Proc. Natl. Acad. Sci. U.S.A. 81*, 7083–7087.

Heberle, J., & Dencher, N. A. (1990) *FEBS Lett. 277* (1, 2), 277–280.

Heberle, J., & Dencher, N. A. (1992) *Proc. Natl. Acad. Sci. U.S.A. 89*, 5996–6000.

Henderson, R., Baldwin, J. M., Ceska, T. A., Zemlin, F., Beckmann, E., & Downing, K. H. (1990) *J. Mol. Biol. 213*, 899–929.

Hess, B., & Kuschmitz, D. (1977) *FEBS Lett. 74* (1), 20–24.

Hildebrandt, P., & Stockburger, M. (1984) *Biochemistry 23*, 5539–5548.

Hofrichter, J., Henry, E. R., & Lozier, R. H. (1989) *Biophys. J. 56*, 693–706.

Holz, M., Drachev, L. A., Mogi, T., Otto, H., Kaulen, A. D., Heyn, M. P., Skulachev, V. P., & Khorana, H. G. (1989) *Proc. Natl. Acad. Sci. U.S.A. 86*, 2167–2171.

Kakitani, H., Kakitani, T., Rodman, H., Honig, B., & Callender, R. (1983) *J. Phys. Chem. 87*, 3620–3628.

Kalisky, O., Lachish, U., & Ottolenghi, M. (1978) *Photochem. Photobiol. 28*, 261–263.

Kalisky, O., Ottolenghi, M., Honig, B., & Korenstein, R. (1981) *Biochemistry 20*, 649–655.

Koch, M. H. J., Dencher, N. A., Oesterhelt, D., Plöhn, H.-J., Rapp, G., & Büldt, G. (1991) *EMBO J. 10* (3), 521–526.

Kouyama, T., Nasuda-Kouyama, A., Ikegami, A., Mathew, M. K., & Stoeckenius, W. (1988) *Biochemistry 27*, 5855–5863.

Lanyi, J. K. (1992) *J. Bioenerg. Biomembr. 24* (2), 169–179.

Li, Q.-Q., Govindjee, R., & Ebrey, T. G. (1984) *Proc. Natl. Acad. Sci. U.S.A. 81*, 7079–7082.

Lohrmann, R., & Stockburger, M. (1992) *J. Raman Spectrosc. 23*, 575–583.

Lohrmann, R., Grieger, I., & Stockburger, M. (1991) *J. Phys. Chem. 95*, 1993–2001.

Lozier, R. H., Bogomolni, R. A., & Stoeckenius, W. (1975) *Biophys. J. 15*, 955–962.

Massig, G., Stockburger, M., & Alshuth, T. (1985) *Can. J. Chem. 63* (7), 2012–2017.

Mathies, R. A., Lin, S. W., Ames, J. B., & Pollard, W. T. (1991) *Annu. Rev. Biophys. Biophys. Chem. 20*, 491–518.
Maurer, R., Vogel, J., & Schneider, S. (1987a) *Photochem. Photobiol. 46* (2), 247–253.
Maurer, R., Vogel, J., & Schneider, S. (1987b) *Photochem. Photobiol. 46* (2), 255–262.
Miller, A., & Oesterhelt, D. (1990) *Biochim. Biophys. Acta 1020*, 57–64.
Mowery, P. C., Lozier, R. H., Chae, Q., Tseng, Y.-W., Taylor, M., & Stoeckenius, W. (1979) *Biochemistry 18*, 4100–4107.
Müller, K.-H., Butt, H. J., Bamberg, E., Fendler, K., Hess, B., Siebert, F., & Engelhard, M. (1991) *Eur. Biophys. J. 19*, 241–251.
Nagle, J., Parodi, L. A., & Lozier, R. H. (1982) *Biophys. J. 38*, 161–174.
Nakagawa, M., Maeda, A., Ogura, T., & Kitagawa, T. (1991) *J. Mol. Struc. 242*, 221–234.
Oesterhelt, D., & Stockenius, W. (1973) *Proc. Natl. Acad. Sci. U.S.A. 70*, 2853–2857.
Oesterhelt, D., & Hess, B. (1973) *Eur. J. Biochem. 37*, 316–326.
Oesterhelt, D., & Stoeckenius, W. (1974) *Methods Enzymol. 31*, 667–678.
Oesterhelt, D., Tittor, J., & Bamberg, E. (1992) *J. Bioenerg. Biomembr. 24* (2), 181–191.
Ohno, K., Takeuchi, Y., & Yoshida, M. (1981) *Photochem. Photobiol. 33*, 573–578.
Olejnik, J., Brzezinski, B., & Zundel, G. (1992) *J. Mol. Struct. 271*, 157–173.
Ormos, P. (1991) *Proc. Natl. Acad. Sci. U.S.A. 88*, 473–477.
Ormos, P., Dancsházy, Z., & Keszthelyi, L. (1980) *Biophys. J. 31*, 207–214.
Ormos, P., Chu, K., & Mourant, J. (1992) *Biochemistry 31*, 6933–6937.
Ort, D. R., & Parson, W. W. (1978) *J. Biol. Chem. 253* (17) 6158–6164.
Ort, D. R., & Parson, W. W. (1979) *Biophys. J. 25*, 355–364.
Otto, H., Marti, T., Holz, M., Mogi, T., Lindau, M., Khorana, H. G., & Heyn, M. P. (1989) *Proc. Natl. Acad. Sci. U.S.A. 86*, 9228–9232.
Otto, H., Marti, T., Holz, M., Mogi, T., Stern, L. J., Engel, F., Khorana, H.-G., & Heyn, M. P. (1990) *Proc. Natl. Acad. Sci. U.S.A. 87*, 1018–1022.
Papadopoulos, G., Dencher, N. A., Zaccai, G., & Büldt, G. (1990) *J. Mol. Biol. 214*, 15–19.
Pfefferlé, J.-M., Maeda, A., Sasaki, J., & Yoshizawa, T. (1991) *Biochemistry 30*, 6548–6556.
Polland, H.-J., Franz, M. A., Zinth, W., Kaiser, W., Kölling, E., & Oesterhelt, D. (1986) *Biophys. J. 49*, 651–662.
Provencher, S. W. (1976) *J. Chem. Phys. 64*, 2772–2777.
Rauen, H. M. (1964) *Biochemisches Taschenbuch*, Springer-Verlag, Berlin.
Rohr, M., Gärtner, W., Schweitzer, G., Holzwarth, A. R., & Braslavsky, S. E. (1992) *J. Phys. Chem. 96*, 6055–6061.
Rothschild, K. J. (1992) *J. Bioenerg. Biomembr. 24* (1), 147–167.
Rothschild, K. J., Braiman, M. S., He, Y.-W., Marti, T., & Khorana, H. G. (1990) *J. Biol. Chem. 265* (28), 16985–16991.
Rothschild, K. J., He, Y.-W., Sanjay, S., Marti, T., & Khorana, H. G. (1992) *J. Biol. Chem. 267* (3), 1615–1622.
Scherrer, P., & Stoeckenius, W. (1985) *Biochemistry 24*, 7733–7740.
Schneider, G., Diller, R., & Stockburger, M. (1989) *Chem. Phys. 131*, 17–29.
Schulten, K., & Tavan, P. (1978) *Nature 272* (5648), 85–86.
Sherman, W. V., Eicke, R. R., Stafford, S. R., & Wasacz, F. M. (1979) *Photochem. Photobiol. 30*, 727–729.
Sheves, M., Albeck, A., Friedman, N., & Ottolenghi, M. (1986) *Proc. Natl. Acad. Sci. U.S.A. 83*, 3262–3266.
Siebert, F., Mäntele, W., & Kreutz, W. (1982) *FEBS Lett. 141* (1), 82–87.
Smith, S. O., Pardoen, J. A., Mulder, P. P. J., Curry, B., Lugtenburg, J., & Mathies, R. (1983) *Biochemistry 22*, 6141–6148.
Stockburger, M., Klusmann, W., Gattermann, H., Massig, G., & Peters, R. (1979) *Biochemistry 18*, 4886–4900.
Stockburger, M., Alshuth, T., Oesterhelt, D., & Gärtner, W. (1986) in *Spectroscopy of Biological Systems* (Clark, R. J. H., & Hester, R. E., Eds.) pp 483–535, John Wiley & Sons, New York.
Stoeckenius, W., & Bogomolni, R. A. (1982) *Annu. Rev. Biochem. 52*, 587–616.
Subramaniam, S., Marti, T., & Khorana, H. G. (1990) *Proc. Natl. Acad. Sci. U.S.A. 87*, 1013–1017.
Tavan, P., Schulten, K., & Oesterhelt, D. (1985) *Biophys. J. 47*, 415–430.
Tittor, J., Soell, C., Oesterhelt, D., Butt, H.-J., & Bamberg, E. (1989) *EMBO J. 8* (11), 3477–3482.
Váró, G., & Lanyi, J. K. (1991a) *Biophys. J. 59*, 313–322.
Váró, G., & Lanyi, J. K. (1991b) *Biochemistry 30*, 5008–5015.
Váró, G., & Lanyi, J. K. (1991c) *Biochemistry 30*, 5016–5022.
Váró, G., Duschl, A., & Lanyi, J. K. (1990) *Biochemistry 29*, 3798–3804.
Wan, Ch., Qian, J., & Johnson, C. K. (1991) *Biochemistry 30*, 394–400.
Xie, A. H., Nagle, J. F., & Lozier, R. H. (1987) *Biophys. J. 51*, 627–635.